

1 Quasi-consistent efficient meshfree thin shell
2 formulation with penalty-free essential boundary
3 condition enforcement

4 Junchao Wu^{a,*}, Yangtao Xu^a, Bin Xu^a, Syed Humayun Basha^a

^a*Key Laboratory for Intelligent Infrastructure and Monitoring of Fujian Province, Key
Laboratory for Structural Engineering and Disaster Prevention of Fujian Province, College
of Civil Engineering, Huaqiao University, Xiamen, Fujian, 361021, China*

5 **Abstract**

This research proposed an efficient and quasi-consistent meshfree thin shell formulation with penalty-free enforcement of essential boundary conditions. Within the framework of the Hu-Washizu variational principle, a mixed formulation of displacements, strains and stresses is employed in this approach, where the displacements are discretized using meshfree shape functions, and the strains and stresses are expressed using smoothed gradients, covariant smoothed gradients and covariant bases. The smoothed gradients satisfy the first second-order integration constraint and have variational consistency for polynomial strains and stresses. Owing to Hu-Washizu variational principle, the essential boundary conditions automatically arise in its weak form. As a result, the suggested technique's enforcement of essential boundary conditions resembles that of the traditional Nitsche's method. Contrary to Nitsche's method, the costly higher order derivatives of conventional meshfree shape functions were replaced by the smoothed gradients with fast computation, which improve the efficiency. Meanwhile, the proposed formulation features a naturally stabilized term without adding any artificial stabilization factors, which eliminates the employment of penalty method as a stabilization. The efficacy of the proposed Hu-Washizu meshfree thin shell formulation is illustrated by a set of classical standard thin shell problems.

6 *Keywords:* Meshfree, Thin shell, Hu-Washizu variational principle,
7 Reproducing kernel gradient smoothing, Essential boundary condition

*Corresponding author
Email address: jcwu@hqu.edu.cn (Junchao Wu)

8 1. Introduction

9 Thin shell structures generally adhere to the Kirchhoff hypothesis [1], that
10 neglects the shear deformation can be described using Galerkin formulation
11 which requires to have at least C^1 continuity. The traditional finite element
12 methods usually only have C^0 continuous shape functions, and it prefers Mindlin
13 thick shear theory, hybrid and mixed models in simulation of shell structure [2].
14 Meshfree methods [3, 4, 5] with high order smoothed shape functions have gar-
15 nered much research attention over the past thirty years. These techniques
16 established the shape functions based on a collection of dispersed nodes, and
17 the high order continuity of shape functions can be easily achieved even with
18 low-order basis functions. For thin shell analysis, this high order meshfree ap-
19 proximation can also alleviate the membrane locking caused by the mismatched
20 approximation order of membrane strain and bending strain [6]. Furthermore,
21 nodal-based meshfree approximations generally offer the flexibility of local re-
22 finement and can relieve the burden of mesh distortion. Owing to these benefits,
23 numerous meshfree techniques have been developed and implemented in many
24 scientific and engineering fields [7, 8, 9, 10, 11, 12, 13]. However, the high order
25 smoothed meshfree shape functions accompany the enlarged and overlapping
26 supports, which may potentially cause many problems for shape functions. One
27 of the issues is the loss of the Kronecker delta property, which means that, un-
28 like the finite element methods, the necessary boundary conditions cannot be
29 directly enforced [14]. Another issue is that the variational consistency or said
30 integration constraint, which is a condition requires the formulation to exactly
31 reproduce the solution spanned by basis functions, cannot be satisfied. This
32 issue is caused by the misalignment between the numerical integration domains
33 and supports of shape functions, and thus, the shape functions exhibit to a
34 piecewise nature in each integration domain. It turns to that the traditional
35 integration rules like Gauss scheme cannot ensure the integration accuracy in
36 Galerkin weak form [15, 16]. Therefore, variational consistency is vital to the
37 solution accuracy in Galerkin formulations.

38 Various ways have been presented to enforce the necessary boundary for
39 Galerkin meshfree methods directly, including the boundary singular kernel
40 method [17], mixed transformation method [17], and interpolation element-free
41 method [18] for recovering shape functions' Kronecker property. However, these
42 methods are not based on a variational setting and cannot guarantee variational
43 consistency. In the absence of a meshfree node, accuracy enforcement might be
44 poorer. In contrast, enforcing the essential boundary conditions using a vari-
45 ational approach is preferred for Galerkin meshfree methods. The variational
46 consistent Lagrange multiplier approach was initially used to the Galerkin mesh-
47 free method by Belytschko et al. [3]. In this method, the extra degrees of free-
48 dom are used to determine the discretion of Lagrange multiplier. Furthermore,
49 Ivannikov et al. [19] have extended this approach to geometrically nonlinear
50 thin shells. Lu et al. [20] suggested the modified variational essential bound-
51 ary enforcement approach and expressed the Lagrange multiplier by equivalent
52 tractions to eliminate the excess degrees of freedom. However, the coercivity

53 of this approach is not always ensured and potentially reduces the accuracy.
 54 Zhu and Atluri [21] pioneered the penalty method for meshfree method, mak-
 55 ing it a straightforward approach to enforce essential boundary conditions via
 56 Galerkin weak form. However, the penalty method lacks variational consistency
 57 and requires experimental artificial parameters whose optimal value is hard to
 58 determine. Fernández-Méndez and Huerta [14] imposed necessary boundary
 59 conditions using Nitsche’s approach in the meshfree formulation. This approach
 60 can be seen as a hybrid combination of the modified variational method and the
 61 penalty method because the modified variational method generates variational
 62 consistency through the use of a consistent term, and the penalty method is
 63 used as a stabilized term to recover the coercivity. Skatulla and Sansour [22]
 64 extended Nitsche’s thin shell analysis method and proposed an iteration algo-
 65 rithm to determine artificial parameters at each integration point.

66 In order to address the issue of numerical integration, a series of consis-
 67 tent integration schemes have been developed for Galerkin meshfree methods.
 68 Among these include stabilized conforming nodal integration [23], variational
 69 consistent integration [24], quadratic consistent integration [25], reproducing
 70 kernel gradient smoothing integration [26], and consistent projection integration
 71 [27]. The assumed strain approach establishes the most consistent integration
 72 scheme, while the smoothed gradient replaces the costly higher order derivatives
 73 of traditional meshfree shape functions and shows a high efficiency. Moreover,
 74 to achieve global variational consistency, a consistent essential boundary con-
 75 dition enforcement should cooperate with the consistent integration scheme.
 76 The consistent integration scheme and Nitsche’s method for treating essential
 77 boundary conditions show a good performance since they can satisfy the coer-
 78 civity without requiring additional degrees of freedom. Nevertheless, Nitsche’s
 79 approach still retains the artificial parameters in stabilized terms, and it is es-
 80 sential to remain conscious of the costly higher order derivatives, particularly
 81 for thin plate and thin shell problems. Recently, Wu et al. [28, 29] proposed
 82 an efficient and stabilized essential boundary condition enforcement method
 83 based upon the Hellinger-Reissner variational principle, where a mixed formu-
 84 lation in Hellinger-Reissner weak form recasts the reproducing kernel gradient
 85 smoothing integration. The terms for enforcing essential boundary conditions
 86 are identical to the Nitsche’s method, and both have consistent and stabilized
 87 terms. Nevertheless, the stabilized term of this method naturally exists in the
 88 Hellinger-Reissner weak form and no longer needs the artificial parameters, even
 89 for essential boundary enforcement; instead all of the higher order derivatives
 90 are represented by smoothed gradients and their derivatives.

91 In this study, an efficient and stabilized variational consistent meshfree
 92 method that naturally enforces the essential boundary conditions is developed
 93 for thin shell structure. Following the concept of the Hellinger-Reissner prin-
 94 ciple base consistent meshfree method, the Hu-Washizu variational principle of
 95 complementary energy with variables of displacement, strains, and stresses is
 96 employed. The displacement is approximated by conventional meshfree shape
 97 functions, and the strains and stresses are expressed by smoothed gradients with
 98 covariant bases. It is important to note that although the first second-order in-

99 tegration requirements are naturally embedded in the smoothed gradients, their
100 fulfillment can only result in a quasi-satisfaction of variational consistency be-
101 cause of the non-polynomial nature of the stresses. Hu-Washizu's weak form is
102 used to evaluate all the essential boundary conditions regarding displacements
103 and rotations. This type of formulation is similar to the Nitsche's method but
104 does not require any artificial parameters. Compared with Nitsche's method,
105 conventional reproducing smoothed gradients and its direct derivatives replace
106 the costly higher order derivatives. By utilizing the advantages of a replicating
107 kernel gradient smoothing framework, the smoothed gradients showed better
108 performance compared to conventional derivatives of shape functions, hence
109 increasing the meshfree formulation's computational efficiency.

110 The remainder of this research paper is structured as follows: The kinematics
111 of the thin shell structure and the weak form of the associated Hu-Washizu
112 principle are briefly described in Section 2. Subsequently, the mixed formulation
113 regarding the displacements, strains and stresses in accordance with Hu-Washizu
114 weak form are presented in Section 3. The discrete equilibrium equations are
115 derived in Section 4 using the naturally occurring accommodation of essential,
116 and they are compared to the equations obtained using Nitsche's method. The
117 numerical results in Section 5 validate the efficacy of the proposed Hu-Washizu
118 meshfree thin shell formulation. Lastly, the concluding remarks are presented
119 in Section 6.

2. Hu-Washizu's formulation of complementary energy for thin shell

2.1. Kinematics for thin shell

Consider the configuration of a shell $\bar{\Omega}$, as shown in Fig. 1, which can be easily described by a parametric curvilinear coordinate system $\boldsymbol{\xi} = \{\xi^i\}_{i=1,2,3}$. The mid-surface of the shell denoted by Ω is specified by the in-plane coordinates $\boldsymbol{\xi} = \{\xi^\alpha\}_{\alpha=1,2}$, as the thickness direction of shell is by ξ^3 , $-\frac{h}{2} \leq \xi^3 \leq \frac{h}{2}$, h is the thickness of shell. In this work, Latin indices take the values from 1 to 3, and Greek indices are evaluated by 1 or 2. For the Kirchhoff hypothesis [6], the position $\mathbf{x} \in \bar{\Omega}$ is defined by linear functions with respect to ξ^3 :

$$\mathbf{x}(\xi^1, \xi^2, \xi^3) = \mathbf{r}(\xi^1, \xi^2) + \xi^3 \mathbf{a}_3(\xi^1, \xi^2) \quad (1)$$

in which \mathbf{r} means the position on the mid-surface of shell, and \mathbf{a}_3 is correspond-

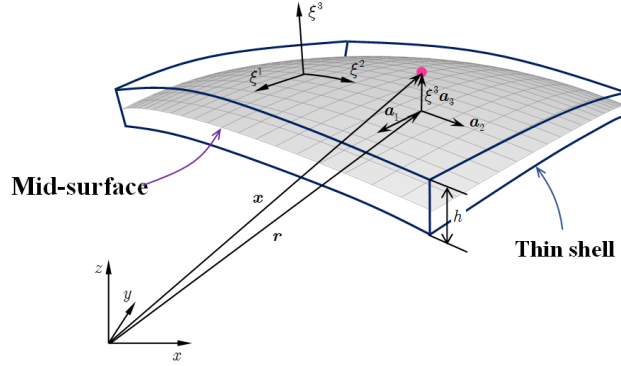


Figure 1: Kinematics for thin shell.

ing normal direction. For the mid-surface of shell, the in-plane covariant base vector with respect to ξ^α can be derived by a trivial partial differentiation to \mathbf{r} :

$$\mathbf{a}_\alpha = \frac{\partial \mathbf{r}}{\partial \xi^\alpha} = \mathbf{r}_{,\alpha}, \alpha = 1, 2 \quad (2)$$

to provide for a clear expression, the subscript comma denotes the partial differentiation operation with respect to in-plane coordinates ξ^α , and the normal vector \mathbf{a}_3 can be obtained by the normalized cross product of \mathbf{a}_α 's as follows:

$$\mathbf{a}_3 = \frac{\mathbf{a}_1 \times \mathbf{a}_2}{\|\mathbf{a}_1 \times \mathbf{a}_2\|} \quad (3)$$

where $\|\bullet\|$ is the Euclidean norm operator.

With the assumption of infinitesimal deformation, the strain components with respect to the global contravariant base can be stated as:

$$\epsilon_{ij} = \frac{1}{2}(\mathbf{x}_{,i} \cdot \mathbf{u}_{,j} + \mathbf{u}_{,i} \cdot \mathbf{x}_{,j}) \quad (4)$$

where \mathbf{u} represents the displacement for the shell deformation. To satisfy the Kirchhoff hypothesis, the displacement is assumed to be of the following form:

$$\mathbf{u}(\xi^1, \xi^2, \xi^3) = \mathbf{v}(\xi^1, \xi^2) + \boldsymbol{\theta}(\xi^1, \xi^2)\xi^3 \quad (5)$$

in which the quadratic and higher order terms are neglected. \mathbf{v} , $\boldsymbol{\theta}$ represent the displacement and rotation in mid-surface, respectively.

Subsequently, plugging Eqs. (1) and (5) into Eq. (4) and neglecting the quadratic terms, the strain components can be rephrased as follows:

$$\begin{aligned} \epsilon_{\alpha\beta} &= \frac{1}{2}(\mathbf{a}_\alpha \cdot \mathbf{v}_{,\beta} + \mathbf{v}_{,\alpha} \cdot \mathbf{a}_\beta) \\ &+ \frac{1}{2}(\mathbf{a}_{3,\alpha} \cdot \mathbf{v}_{,\beta} + \mathbf{v}_{,\alpha} \cdot \mathbf{a}_{3,\beta} + \mathbf{a}_\alpha \cdot \boldsymbol{\theta}_{,\beta} + \boldsymbol{\theta}_{,\alpha} \cdot \mathbf{a}_\beta)\xi^3 \\ &= \varepsilon_{\alpha\beta} + \kappa_{\alpha\beta}\xi^3 \end{aligned} \quad (6a)$$

$$\epsilon_{\alpha 3} = \frac{1}{2}(\mathbf{a}_\alpha \cdot \boldsymbol{\theta} + \mathbf{v}_{,\alpha} \cdot \mathbf{a}_3) + \frac{1}{2}(\mathbf{a}_3 \cdot \boldsymbol{\theta})_{,\alpha}\xi^3 \quad (6b)$$

$$\epsilon_{33} = \mathbf{a}_3 \cdot \boldsymbol{\theta} \quad (6c)$$

where $\varepsilon_{\alpha\beta}$, $\kappa_{\alpha\beta}$ represent membrane and bending strains, respectively, and are given as follows:

$$\varepsilon_{\alpha\beta} = \frac{1}{2}(\mathbf{a}_\alpha \cdot \mathbf{v}_{,\beta} + \mathbf{v}_{,\alpha} \cdot \mathbf{a}_\beta) \quad (7)$$

$$\kappa_{\alpha\beta} = \frac{1}{2}(\mathbf{a}_{3,\alpha} \cdot \mathbf{v}_{,\beta} + \mathbf{v}_{,\alpha} \cdot \mathbf{a}_{3,\beta} + \mathbf{a}_\alpha \cdot \boldsymbol{\theta}_{,\beta} + \boldsymbol{\theta}_{,\alpha} \cdot \mathbf{a}_\beta) \quad (8)$$

In accordance with the Kirchhoff hypothesis, the thickness of shell will not change, and the deformation related with direction of ξ^3 will vanish, i.e. $\epsilon_{3i} = 0$. Thus, the rotation $\boldsymbol{\theta}$ can be rewritten as:

$$\epsilon_{3i} = 0 \Rightarrow \begin{cases} \boldsymbol{\theta} \cdot \mathbf{a}_\alpha = -\mathbf{v}_{,\alpha} \cdot \mathbf{a}_3 \\ \boldsymbol{\theta} \cdot \mathbf{a}_3 = 0 \end{cases} \Rightarrow \boldsymbol{\theta} = -\mathbf{v}_{,\alpha} \cdot \mathbf{a}_3 \mathbf{a}^\alpha \quad (9)$$

where \mathbf{a}^α 's is the in-plane contravariant base vector, $\mathbf{a}^\alpha \cdot \mathbf{a}_\beta = \delta_\beta^\alpha$, δ is the Kronecker delta function. The detailed derivation of Eq. 9 can be found in reference [30].

Furthermore, substituting Eq. (9) into Eq. (8) leads to:

$$\kappa_{\alpha\beta} = (\Gamma_{\alpha\beta}^\gamma \mathbf{v}_{,\gamma} - \mathbf{v}_{,\alpha\beta}) \cdot \mathbf{a}_3 = -\mathbf{v}_{,\alpha}|_\beta \cdot \mathbf{a}_3 \quad (10)$$

in which $\Gamma_{\alpha\beta}^\gamma = \mathbf{a}_{\alpha,\beta} \cdot \mathbf{a}^\gamma$ is namely the Christoffel symbol of the second kind, and $\mathbf{v}_{,\alpha}|_\beta$ is the in-plane covariant derivative of $\mathbf{v}_{,\alpha}$, i.e. $\mathbf{v}_{,\alpha}|_\beta = \Gamma_{\alpha\beta}^\gamma \mathbf{v}_{,\gamma} - \mathbf{v}_{,\alpha\beta}$.

2.2. Galerkin weak form for Hu-Washizu principle of complementary energy

In this study, the Hu-Washizu variational principle of complementary energy [31] was adopted for the development of the proposed analytical approach, the

159 corresponding complementary functional, denoted by Π_C , is listed as follows:

$$\begin{aligned}
& \Pi_C(\varepsilon_{\alpha\beta}, \kappa_{\alpha\beta}, N^{\alpha\beta}, M^{\alpha\beta}) \\
&= \int_{\Omega} \frac{h}{2} \varepsilon_{\alpha\beta} C^{\alpha\beta\gamma\eta} \varepsilon_{\gamma\eta} d\Omega + \int_{\Omega} \frac{h^3}{24} \kappa_{\alpha\beta} C^{\alpha\beta\gamma\eta} \kappa_{\gamma\eta} d\Omega \\
&+ \int_{\Omega} \varepsilon_{\alpha\beta} (N^{\alpha\beta} - h C^{\alpha\beta\gamma\eta} \varepsilon_{\gamma\eta}) d\Omega + \int_{\Omega} \kappa_{\alpha\beta} (M^{\alpha\beta} - \frac{h^3}{12} C^{\alpha\beta\gamma\eta} \kappa_{\gamma\eta}) d\Omega \quad (11) \\
&- \int_{\Gamma_v} \mathbf{T} \cdot \bar{\mathbf{v}} d\Gamma + \int_{\Gamma_{\theta}} M_{\mathbf{n}\mathbf{n}} \bar{\theta}_{\mathbf{n}} d\Gamma - (P \mathbf{a}_3 \cdot \bar{\mathbf{v}})_{\mathbf{x} \in C_w}
\end{aligned}$$

160 where $C^{\alpha\beta\gamma\eta}$'s represent the components of fourth order elasticity tensor with
161 respect to the covariant base and plane stress assumption, and it can be ex-
162 pressed by Young's modulus E , Poisson's ratio ν and the in-plane contravariant
163 metric coefficients $a^{\alpha\beta}$'s, $a^{\alpha\beta} = \mathbf{a}^{\alpha} \cdot \mathbf{a}^{\beta}$, as follows:

$$C^{\alpha\beta\gamma\eta} = \frac{E}{2(1+\nu)} (a^{\alpha\gamma} a^{\beta\eta} + a^{\alpha\eta} a^{\beta\gamma} + \frac{2\nu}{1-\nu} a^{\alpha\beta} a^{\gamma\eta}) \quad (12)$$

164 and $N^{\alpha\beta}$, $M^{\alpha\beta}$ are the components of membrane and bending stresses given by:

$$N^{\alpha\beta} = h C^{\alpha\beta\gamma\eta} \varepsilon_{\gamma\eta}, \quad M^{\alpha\beta} = \frac{h^3}{12} C^{\alpha\beta\gamma\eta} \kappa_{\gamma\eta} \quad (13)$$

165 Essential boundaries on the edges and corners denoted by Γ_v , Γ_{θ} and C_v
166 are naturally existed in complementary energy functional, $\bar{\mathbf{v}}$, $\bar{\theta}_{\mathbf{n}}$ are the cor-
167 responding prescribed displacement and normal rotation, respectively. \mathbf{T} , $M_{\mathbf{n}\mathbf{n}}$
168 and P can be determined by Euler-Lagrange equations of shell problem [30] as
169 follows:

$$\mathbf{T} = \mathbf{T}_N + \mathbf{T}_M \rightarrow \begin{cases} \mathbf{T}_N = \mathbf{a}_{\alpha} N^{\alpha\beta} n_{\beta} \\ \mathbf{T}_M = (\mathbf{a}_3 M^{\alpha\beta} s_{\alpha} n_{\beta})_{,\gamma} s^{\gamma} + (\mathbf{a}_3 M^{\alpha\beta})_{|\beta} n_{\alpha} \end{cases} \quad (14)$$

$$M_{\mathbf{n}\mathbf{n}} = M^{\alpha\beta} n_{\alpha} n_{\beta} \quad (15)$$

$$P = -[[M^{\alpha\beta} s_{\alpha} n_{\beta}]] \quad (16)$$

172 where $\mathbf{n} = n^{\alpha} \mathbf{a}_{\alpha} = n_{\alpha} \mathbf{a}^{\alpha}$ and $\mathbf{s} = s^{\alpha} \mathbf{a}_{\alpha} = s_{\alpha} \mathbf{a}^{\alpha}$ are the outward normal and
173 tangent directions on boundaries. $[[f]]$ is the jump operator defined by:

$$[[f]]_{\mathbf{x}=\mathbf{x}_c} = \lim_{\epsilon \rightarrow \mathbf{0}^+} (f(\mathbf{x}_c + \epsilon) - f(\mathbf{x}_c - \epsilon)), \mathbf{x}_c \in \Gamma \quad (17)$$

174 where f is an arbitrary function on Γ .

175 Moreover, the natural boundary conditions should be applied by Lagrangian
176 multiplier method with displacement \mathbf{v} regarded as multiplier. Thus, then the
177 new complementary energy functional namely Π is given by:

$$\begin{aligned}
& \Pi(\mathbf{v}, \varepsilon_{\alpha\beta}, \kappa_{\alpha\beta}, N^{\alpha\beta}, M^{\alpha\beta}) \\
&= \Pi_C(\varepsilon_{\alpha\beta}, \kappa_{\alpha\beta}, N^{\alpha\beta}, M^{\alpha\beta}) + \int_{\Gamma_M} \theta_{\mathbf{n}} (M_{\mathbf{n}\mathbf{n}} - \bar{M}_{\mathbf{n}\mathbf{n}}) d\Gamma \quad (18) \\
&- \int_{\Gamma_T} \mathbf{v} \cdot (\mathbf{T} - \bar{\mathbf{T}}) d\Gamma - \mathbf{v} \cdot \mathbf{a}_3 (P - \bar{P})_{\mathbf{x} \in C_P} - \int_{\Omega} \mathbf{v} \cdot (\mathbf{b} - \bar{\mathbf{b}}) d\Omega
\end{aligned}$$

178 where $\bar{\mathbf{T}}$, \bar{M}_{nn} and \bar{P} are the prescribed traction, bending moment and concen-
 179 trated force on edges Γ_T , Γ_M and corner C_P respectively. All the boundaries
 180 meet the following geometric relationships:

$$\begin{cases} \Gamma = \Gamma_v \cup \Gamma_T \cup \Gamma_\theta \cup \Gamma_M, & C = C_v \cup C_P, \\ \Gamma_v \cap \Gamma_T = \Gamma_\theta \cap \Gamma_M = C_v \cap C_P = \emptyset \end{cases} \quad (19)$$

181 and $\bar{\mathbf{b}}$ stands for the prescribed body force in Ω , \mathbf{b} also can be written based on
 182 Euler-Lagrange equations [30] as:

$$\mathbf{b} = \mathbf{b}_N + \mathbf{b}_M \rightarrow \begin{cases} \mathbf{b}_N = (\mathbf{a}_\alpha N^{\alpha\beta})|_\beta \\ \mathbf{b}_M = (\mathbf{a}_3 M^{\alpha\beta})|_{\alpha\beta} \end{cases} \quad (20)$$

183 Introducing a standard variational argument to Eq. (18), $\delta\Pi = 0$, and
 184 considering the arbitrariness of virtual variables, $\delta\mathbf{v}$, $\delta\varepsilon_{\alpha\beta}$, $\delta\kappa_{\alpha\beta}$, $N^{\alpha\beta}$, $M^{\alpha\beta}$
 185 lead to the following weak form:

$$-\int_{\Omega} h\delta\varepsilon_{\alpha\beta} C^{\alpha\beta\gamma\eta} \varepsilon_{\gamma\eta} d\Omega + \int_{\Omega} \delta\varepsilon_{\alpha\beta} N^{\alpha\beta} d\Omega = 0 \quad (21a)$$

$$-\int_{\Omega} \frac{h^3}{12} \delta\kappa_{\alpha\beta} C^{\alpha\beta\gamma\eta} \kappa_{\gamma\eta} d\Omega + \int_{\Omega} \delta\kappa_{\alpha\beta} M^{\alpha\beta} d\Omega = 0 \quad (21b)$$

$$\begin{aligned} \int_{\Omega} \delta N^{\alpha\beta} \varepsilon_{\alpha\beta} d\Omega - \int_{\Gamma} \delta \mathbf{T}_N \cdot \mathbf{v} d\Gamma + \int_{\Omega} \delta \mathbf{b}_N \cdot \mathbf{v} d\Omega \\ + \int_{\Gamma_v} \delta \mathbf{T}_N \cdot \mathbf{v} d\Gamma = \int_{\Gamma_v} \delta \mathbf{T}_N \cdot \bar{\mathbf{v}} d\Gamma \end{aligned} \quad (21c)$$

$$\begin{aligned} \int_{\Omega} \delta M^{\alpha\beta} \kappa_{\alpha\beta} d\Omega - \int_{\Gamma} \delta M_{nn} \theta_n d\Gamma + \int_{\Gamma} \delta \mathbf{T}_M \cdot \mathbf{v} d\Gamma + (\delta P \mathbf{a}_3 \cdot \mathbf{v})_{\mathbf{x} \in C} + \int_{\Omega} \delta \mathbf{b}_M \cdot \mathbf{v} d\Omega \\ + \int_{\Gamma_\theta} \delta M_{nn} \theta_n d\Gamma - \int_{\Gamma_v} \delta \mathbf{T}_M \cdot \mathbf{v} d\Gamma - (\delta P \mathbf{a}_3 \cdot \mathbf{v})_{\mathbf{x} \in C_v} \\ = \int_{\Gamma_\theta} \delta M_{nn} \bar{\theta}_n d\Gamma - \int_{\Gamma_v} \delta \mathbf{T}_M \cdot \bar{\mathbf{v}} d\Gamma - (\delta P \mathbf{a}_3 \cdot \bar{\mathbf{v}})_{\mathbf{x} \in C_v} \end{aligned} \quad (21d)$$

$$\begin{aligned} \int_{\Gamma} \delta \theta_n M_{nn} d\Gamma - \int_{\Gamma} \delta \mathbf{v} \cdot \mathbf{T} d\Gamma - (\delta \mathbf{v} \cdot \mathbf{a}_3 P)_{\mathbf{x} \in C} + \int_{\Omega} \delta \mathbf{v} \cdot \mathbf{b} d\Omega \\ - \int_{\Gamma_\theta} \delta \theta_n M_{nn} d\Gamma + \int_{\Gamma_v} \delta \mathbf{v} \cdot \mathbf{T} d\Gamma + (\delta \mathbf{v} \cdot \mathbf{a}_3 P)_{\mathbf{x} \in C_v} = - \int_{\Gamma_T} \delta \mathbf{v} \cdot \bar{\mathbf{t}} d\Gamma - \int_{\Omega} \delta \mathbf{v} \cdot \bar{\mathbf{b}} d\Omega \end{aligned} \quad (21e)$$

190 where the geometric relationships of Eq. (19) is used herein.

191 **3. Mixed meshfree formulation for modified Hellinger-Reissner weak** 192 **form**

193 *3.1. Reproducing kernel approximation for displacement*

194 This study approximates the displacement by adopting reproducing kernel
195 approximation. As shown in Fig. 2, the mid-surface of the shell Ω is discretized
196 by a set of meshfree nodes $\{\boldsymbol{\xi}_I\}_{I=1}^{n_p}$ in parametric configuration, where n_p is the
197 total number of meshfree nodes. The approximated displacement namely \mathbf{v}^h
198 can be expressed as:

$$\mathbf{v}(\boldsymbol{\xi}) = \sum_{I=1}^{n_p} \Psi_I(\boldsymbol{\xi}) \mathbf{d}_I \quad (22)$$

199 in which Ψ_I and \mathbf{d}_I is the shape function and nodal coefficient tensor related by
200 node $\boldsymbol{\xi}_I$. According to reproducing kernel approximation [4], the shape function
201 takes the following form:

$$\Psi_I(\boldsymbol{\xi}) = \mathbf{p}^T(\boldsymbol{\xi}) \mathbf{c}(\boldsymbol{\xi}) \phi(\boldsymbol{\xi}_I - \boldsymbol{\xi}) \quad (23)$$

202 where \mathbf{p} is the basis function vector represented using the following quadratic
203 function as:

$$\mathbf{p} = \{1, \xi^1, \xi^2, (\xi^1)^2, \xi^1 \xi^2, (\xi^2)^2\}^T \quad (24)$$

204 The kernel function denoted by ϕ controls the support and smoothness of
205 meshfree shape functions. The quintic B-spline function with square support is
206 used herein as the kernel function:

$$\phi(\boldsymbol{\xi}_I - \boldsymbol{\xi}) = \phi(\hat{s}_1) \phi(\hat{s}_2), \quad \hat{s}_\alpha = \frac{|\xi_I^\alpha - \xi^\alpha|}{s_{\alpha I}} \quad (25)$$

207 with

$$\phi(\hat{s}_\alpha) = \frac{1}{5!} \begin{cases} (3 - 3\hat{s}_\alpha)^5 - 6(2 - 3\hat{s}_\alpha)^5 + 15(1 - 3\hat{s}_\alpha)^5 & \hat{s}_\alpha \leq \frac{1}{3} \\ (3 - 3\hat{s}_\alpha)^5 - 6(2 - 3\hat{s}_\alpha)^5 & \frac{1}{3} < \hat{s}_\alpha \leq \frac{2}{3} \\ (3 - 3\hat{s}_\alpha)^5 & \frac{2}{3} < \hat{s}_\alpha \leq 1 \\ 0 & \hat{s}_\alpha > 1 \end{cases} \quad (26)$$

208 and $s_{\alpha I}$ means the support size of meshfree shape function Ψ_I .

209 The unknown vector \mathbf{c} in shape function are determined by the fulfillment
210 of the so-called consistency condition:

$$\sum_{I=1}^{n_p} \Psi_I(\boldsymbol{\xi}) \mathbf{p}(\boldsymbol{\xi}_I) = \mathbf{p}(\boldsymbol{\xi}) \quad (27)$$

211 or equivalently

$$\sum_{I=1}^{n_p} \Psi_I(\boldsymbol{\xi}) \mathbf{p}(\boldsymbol{\xi}_I - \boldsymbol{\xi}) = \mathbf{p}(\mathbf{0}) \quad (28)$$

212 Substituting Eq. (22) into (28), yields:

$$\mathbf{A}(\boldsymbol{\xi})\mathbf{c}(\boldsymbol{\xi}) = \mathbf{p}(\mathbf{0}) \quad \Rightarrow \quad \mathbf{c}(\boldsymbol{\xi}) = \mathbf{A}^{-1}(\boldsymbol{\xi})\mathbf{p}(\mathbf{0}) \quad (29)$$

213 where \mathbf{A} is the moment matrix:

$$\mathbf{A}(\boldsymbol{\xi}) = \sum_{I=1}^{n_p} \phi(\boldsymbol{\xi}_I - \boldsymbol{\xi}) \mathbf{p}(\boldsymbol{\xi}_I - \boldsymbol{\xi}) \mathbf{p}^T(\boldsymbol{\xi}_I - \boldsymbol{\xi}) \quad (30)$$

214 Substituting Eq. (29) back into Eq. (22), the expression of meshfree shape
215 function can be written as:

$$\Psi_I(\boldsymbol{\xi}) = \mathbf{p}^T(\boldsymbol{\xi}_I - \boldsymbol{\xi}) \mathbf{A}^{-1}(\boldsymbol{\xi}) \mathbf{p}(\mathbf{0}) \phi(\boldsymbol{\xi}_I - \boldsymbol{\xi}) \quad (31)$$

216 3.2. Reproducing kernel gradient smoothing approximation for effective stress 217 and strain

218 In Galerkin meshfree formulation, the mid-plane of thin shell Ω is split by
219 a set of integration cells Ω_C 's, $\cup_{C=1}^{n_e} \Omega_C \approx \Omega$, as shown in Fig. 2. With the
220 inspiration of reproducing kernel smoothing framework, the Cartesian and co-
221 variant derivatives of displacement, $\mathbf{v}_{,\alpha}$ and $-\mathbf{v}_{,\alpha}|_{\beta}$, in strains $\varepsilon_{\alpha\beta}$, $\kappa_{\alpha\beta}$ are
222 approximated by $(p-1)$ -th order polynomials in each integration cells. In inte-
223 gration cell Ω_C , the approximated derivatives and strains denoted by $\mathbf{v}_{,\alpha}^h$, $\varepsilon_{\alpha\beta}^h$
224 and $-\mathbf{v}_{,\alpha}^h|_{\beta}$, $\kappa_{\alpha\beta}^h$ can be expressed by:

$$\mathbf{v}_{,\alpha}^h(\boldsymbol{\xi}) = \mathbf{q}^T(\boldsymbol{\xi}) \mathbf{d}_{\alpha}^{\varepsilon}, \quad \varepsilon_{\alpha\beta}^h(\boldsymbol{\xi}) = \mathbf{q}^T(\boldsymbol{\xi}) \frac{1}{2} (\mathbf{a}_{\alpha} \cdot \mathbf{d}_{\beta}^{\varepsilon} + \mathbf{a}_{\beta} \cdot \mathbf{d}_{\alpha}^{\varepsilon}) \quad (32)$$

$$-\mathbf{v}_{,\alpha}^h|_{\beta}(\boldsymbol{\xi}) = \mathbf{q}^T(\boldsymbol{\xi}) \mathbf{d}_{\alpha\beta}^{\kappa}, \quad \kappa_{\alpha\beta}^h(\boldsymbol{\xi}) = \mathbf{q}^T(\boldsymbol{\xi}) \mathbf{a}_3 \cdot \mathbf{d}_{\alpha\beta}^{\kappa} \quad (33)$$

226 where \mathbf{q} is the linear polynomial vector and has the following form:

$$\mathbf{q} = \{1, \xi^1, \xi^2\}^T \quad (34)$$

227 and the $\mathbf{d}_{\alpha}^{\varepsilon}$, $\mathbf{d}_{\alpha\beta}^{\kappa}$ are the corresponding coefficient vector tensors. For the con-
228 ciseness, the mixed usage of tensor and vector is introduced in this study. For
229 instance, the component of coefficient tensor vector $\mathbf{d}_{\alpha I}^{\varepsilon}$, $\mathbf{d}_{\alpha}^{\varepsilon} = \{\mathbf{d}_{\alpha I}^{\varepsilon}\}$, is a three
230 dimensional tensor, $\dim \mathbf{d}_{\alpha I}^{\varepsilon} = \dim \mathbf{v}$.

231 In order to meet the integration constraint of thin shell problem, the ap-
232 proximated stresses $N^{\alpha\beta h}$, $M^{\alpha\beta h}$ are assumed to be a similar form with strains,
233 yields:

$$N^{\alpha\beta h}(\boldsymbol{\xi}) = \mathbf{q}^T(\boldsymbol{\xi}) \mathbf{a}^{\alpha} \cdot \mathbf{d}_N^{\beta}, \quad \mathbf{a}_{\alpha} N^{\alpha\beta h}(\boldsymbol{\xi}) = \mathbf{q}^T(\boldsymbol{\xi}) \mathbf{d}_N^{\beta} \quad (35)$$

$$M^{\alpha\beta h}(\boldsymbol{\xi}) = \mathbf{q}^T(\boldsymbol{\xi}) \mathbf{a}_3 \cdot \mathbf{d}_M^{\alpha\beta}, \quad \mathbf{a}_3 M^{\alpha\beta h}(\boldsymbol{\xi}) = \mathbf{q}^T(\boldsymbol{\xi}) \mathbf{d}_M^{\alpha\beta} \quad (36)$$

235 substituting the approximations of Eqs. (22), (32), (33), (35), (36) into Eqs.
236 (21c), (21d) can express $\mathbf{d}_{\beta}^{\varepsilon}$ and $\mathbf{d}_{\alpha\beta}^{\kappa}$ by \mathbf{d} as:

$$\mathbf{d}_{\beta}^{\varepsilon} = \mathbf{G}^{-1} \left(\sum_{I=1}^{n_p} (\tilde{\mathbf{g}}_{\beta I} - \bar{\mathbf{g}}_{\beta I}) \mathbf{d}_I + \hat{\mathbf{g}}_{\beta} \right) \quad (37)$$

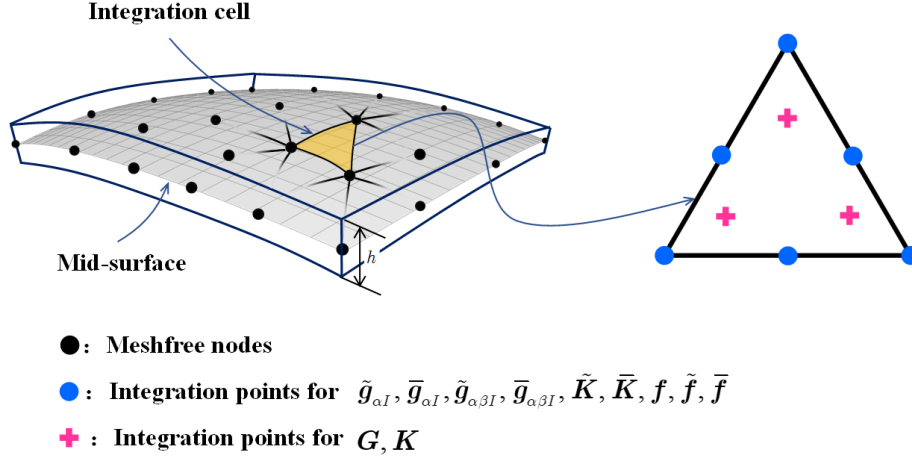


Figure 2: Integration scheme for Hu-Washizu weak form.

$$d_{\alpha\beta}^{\kappa} = G^{-1} \left(\sum_{I=1}^{n_p} (\tilde{g}_{\alpha\beta I} - \bar{g}_{\alpha\beta I}) d_I + \hat{g}_{\alpha\beta} \right) \quad (38)$$

with

$$G = \int_{\Omega_C} q^T q d\Omega \quad (39)$$

$$\tilde{g}_{\beta I} = \int_{\Gamma_C} \Psi_I q n_{\beta} d\Gamma - \int_{\Omega_C} \Psi_I q_{|\beta} d\Omega \quad (40a)$$

$$\bar{g}_{\beta I} = \int_{\Gamma_C \cap \Gamma_v} \Psi_I q n_{\beta} d\Gamma \quad (40b)$$

$$\hat{g}_{\beta} = \int_{\Gamma_C \cap \Gamma_v} q n_{\beta} \bar{v} d\Gamma \quad (40c)$$

$$\begin{aligned} \tilde{g}_{\alpha\beta I} = & \int_{\Gamma_C} \Psi_{I,\gamma} n^{\gamma} q n_{\alpha} n_{\beta} d\Gamma - \int_{\Gamma_C} \Psi_I (q_{|\beta} n_{\alpha} + (q s_{\alpha} n_{\beta})_{,\gamma} s^{\gamma}) d\Gamma \\ & + [[\Psi_I q s_{\alpha} n_{\beta}]]_{\mathbf{x} \in C_C} - \int_{\Omega_C} \Psi q_{,\alpha|\beta} d\Omega \end{aligned} \quad (41a)$$

$$\begin{aligned} \bar{g}_{\alpha\beta I} = & \int_{\Gamma_C \cap \Gamma_{\theta}} \Psi_{I,\gamma} n^{\gamma} q n_{\alpha} n_{\beta} d\Gamma - \int_{\Gamma_C \cap \Gamma_v} \Psi_I (q_{|\beta} n_{\alpha} + (q s_{\alpha} n_{\beta})_{,\gamma} s^{\gamma}) d\Gamma \\ & + [[\Psi_I q s_{\alpha} n_{\beta}]]_{\mathbf{x} \in C_C \cap C_v} \end{aligned} \quad (41b)$$

$$\begin{aligned} \hat{g}_{\alpha\beta} = & \int_{\Gamma_C \cap \Gamma_{\theta}} q n_{\alpha} n_{\beta} a_3 \bar{\theta}_{\mathbf{n}} d\Gamma - \int_{\Gamma_C \cap \Gamma_v} (q_{|\beta} n_{\alpha} + (q s_{\alpha} n_{\beta})_{,\gamma} s^{\gamma}) \bar{v} d\Gamma \\ & + [[q s_{\alpha} n_{\beta} \bar{v}]]_{\mathbf{x} \in C_C \cap C_v} \end{aligned} \quad (41c)$$

241 where evaluations of $\mathbf{q}_{|\beta}$, $\mathbf{q}_{,\alpha|\beta}$ are detail in Appendix A. Further plugging Eqs.
 242 (37) and (38) back into Eqs. (32) and (33) respectively gives the final expression
 243 of $\mathbf{v}_{,\alpha}^h$, $\varepsilon_{\alpha\beta}^h$ and $-\mathbf{v}_{,\alpha\beta}^h$, $\kappa_{\alpha\beta}^h$ as:

$$\mathbf{v}_{,\alpha}^h = \sum_{I=1}^{n_p} (\tilde{\Psi}_{I,\alpha} - \bar{\Psi}_{I,\alpha}) \mathbf{d}_I + \mathbf{q}^T \mathbf{G}^{-1} \hat{\mathbf{g}}_\alpha \quad (42a)$$

$$\begin{aligned} \varepsilon_{\alpha\beta}^h &= \sum_{I=1}^{n_p} \frac{1}{2} (\mathbf{a}_\alpha \tilde{\Psi}_{I,\beta} + \mathbf{a}_\beta \tilde{\Psi}_{I,\alpha}) \cdot \mathbf{d}_I - \sum_{I=1}^{n_p} \frac{1}{2} (\mathbf{a}_\alpha \bar{\Psi}_{I,\beta} + \mathbf{a}_\beta \bar{\Psi}_{I,\alpha}) \cdot \mathbf{d}_I \\ &\quad + \mathbf{q}^T \mathbf{G}^{-1} \frac{1}{2} (\mathbf{a}_\alpha \cdot \hat{\mathbf{g}}_\beta + \mathbf{a}_\beta \cdot \hat{\mathbf{g}}_\alpha) \\ &= \tilde{\varepsilon}_{\alpha\beta}^h - \bar{\varepsilon}_{\alpha\beta}^h + \hat{\varepsilon}_{\alpha\beta}^h \end{aligned} \quad (42b)$$

$$-\mathbf{v}_{,\alpha\beta}^h = \sum_{I=1}^{n_p} (\tilde{\Psi}_{I,\alpha\beta} - \bar{\Psi}_{I,\alpha\beta}) \mathbf{d}_I + \mathbf{q}^T \mathbf{G}^{-1} \hat{\mathbf{g}}_{\alpha\beta} \quad (43a)$$

$$\begin{aligned} \kappa_{\alpha\beta}^h &= \sum_{I=1}^{n_p} \tilde{\Psi}_{I,\alpha\beta} \mathbf{a}_3 \cdot \mathbf{d}_I - \sum_{I=1}^{n_p} \bar{\Psi}_{I,\alpha\beta} \mathbf{a}_3 \cdot \mathbf{d}_I + \mathbf{q}^T \mathbf{G}^{-1} \mathbf{a}_3 \cdot \hat{\mathbf{g}}_{\alpha\beta} \\ &= \tilde{\kappa}_{\alpha\beta}^h - \bar{\kappa}_{\alpha\beta}^h + \hat{\kappa}_{\alpha\beta}^h \end{aligned} \quad (43b)$$

247 with

$$\begin{cases} \tilde{\varepsilon}_{\alpha\beta}^h = \sum_{I=1}^{n_p} \frac{1}{2} (\mathbf{a}_\alpha \tilde{\Psi}_{I,\beta} + \mathbf{a}_\beta \tilde{\Psi}_{I,\alpha}) \cdot \mathbf{d}_I = \sum_{I=1}^{n_p} \tilde{\varepsilon}_{\alpha\beta I} \cdot \mathbf{d}_I \\ \bar{\varepsilon}_{\alpha\beta}^h = \sum_{I=1}^{n_p} \frac{1}{2} (\mathbf{a}_\alpha \bar{\Psi}_{I,\beta} + \mathbf{a}_\beta \bar{\Psi}_{I,\alpha}) \cdot \mathbf{d}_I = \sum_{I=1}^{n_p} \bar{\varepsilon}_{\alpha\beta I} \cdot \mathbf{d}_I \\ \hat{\varepsilon}_{\alpha\beta}^h = \mathbf{q}^T \mathbf{G}^{-1} \frac{1}{2} (\mathbf{a}_\alpha \cdot \hat{\mathbf{g}}_\beta + \mathbf{a}_\beta \cdot \hat{\mathbf{g}}_\alpha) \end{cases} \quad (44)$$

$$\begin{cases} \tilde{\Psi}_{I,\alpha}(\boldsymbol{\xi}) = \mathbf{q}^T(\boldsymbol{\xi}) \mathbf{G}^{-1} \tilde{\mathbf{g}}_{\alpha I} \\ \bar{\Psi}_{I,\alpha}(\boldsymbol{\xi}) = \mathbf{q}^T(\boldsymbol{\xi}) \mathbf{G}^{-1} \bar{\mathbf{g}}_{\alpha I} \\ \tilde{\varepsilon}_{\alpha\beta I} = \frac{1}{2} (\mathbf{a}_\alpha \tilde{\Psi}_{I,\beta} + \mathbf{a}_\beta \tilde{\Psi}_{I,\alpha}) \\ \bar{\varepsilon}_{\alpha\beta I} = \frac{1}{2} (\mathbf{a}_\alpha \bar{\Psi}_{I,\beta} + \mathbf{a}_\beta \bar{\Psi}_{I,\alpha}) \end{cases} \quad (45)$$

$$\begin{cases} \tilde{\kappa}_{\alpha\beta}^h = \sum_{I=1}^{n_p} \tilde{\Psi}_{I,\alpha\beta} \mathbf{a}_3 \cdot \mathbf{d}_I = \sum_{I=1}^{n_p} \tilde{\kappa}_{\alpha\beta I} \cdot \mathbf{d}_I \\ \bar{\kappa}_{\alpha\beta}^h = \sum_{I=1}^{n_p} \bar{\Psi}_{I,\alpha\beta} \mathbf{a}_3 \cdot \mathbf{d}_I = \sum_{I=1}^{n_p} \bar{\kappa}_{\alpha\beta I} \cdot \mathbf{d}_I \\ \hat{\kappa}_{\alpha\beta}^h = \mathbf{q}^T \mathbf{G}^{-1} \mathbf{a}_3 \cdot \hat{\mathbf{g}}_{\alpha\beta} \end{cases} \quad (46)$$

$$\begin{cases} \tilde{\Psi}_{I,\alpha\beta}(\boldsymbol{\xi}) = \mathbf{q}^T(\boldsymbol{\xi})\mathbf{G}^{-1}\tilde{\mathbf{g}}_{\alpha\beta I} \\ \bar{\Psi}_{I,\alpha\beta}(\boldsymbol{\xi}) = \mathbf{q}^T(\boldsymbol{\xi})\mathbf{G}^{-1}\tilde{\mathbf{g}}_{\alpha\beta I} \\ \tilde{\boldsymbol{\kappa}}_{\alpha\beta I} = \tilde{\Psi}_{I,\alpha\beta}\mathbf{a}_3 \\ \bar{\boldsymbol{\kappa}}_{\alpha\beta I} = \bar{\Psi}_{I,\alpha\beta}\mathbf{a}_3 \end{cases} \quad (47)$$

251 It has to be noted that, referring to reproducing kernel gradient smoothing
 252 framework [26], $\tilde{\Psi}_{I,\alpha}$, $\tilde{\Psi}_{I,\alpha\beta}$ are actually the first and second order smoothed
 253 gradients in curvilinear coordinates. $\tilde{\mathbf{g}}_{\alpha I}$ and $\tilde{\mathbf{g}}_{\alpha\beta I}$ are the right hand side in-
 254 tegration constraints for first and second order gradients, then this formulation
 255 can meet the variational consistency for the second order polynomials. It should
 256 be known that, in curved model, the variational consistency for non-polynomial
 257 functions, like trigonometric functions, should be required for the polynomial
 258 solution. Even with high order polynomial variational consistency, the proposed
 259 formulation can not exactly reproduce the solution spanned by basis functions.
 260 However, the accuracy of reproducing kernel smoothed gradients is still better
 261 than traditional meshfree formulation. Numerical examples in the section below
 262 will provide better evidence to prove the accuracy of the reproducing kernel
 263 smoothed gradients.

264 **4. Naturally variational enforcement for essential boundary condi-**
 265 **tions**

266 *4.1. Discrete equilibrium equations*

267 With the approximated effective stresses and strains, the last equation of
 268 weak form Eq. (21e) becomes:

$$-\sum_{C=1}^{n_e} \sum_{I=1}^{n_p} \delta \mathbf{d}_I \cdot \left((\tilde{\mathbf{g}}_{\alpha I}^T - \bar{\mathbf{g}}_{\alpha I}^T) \mathbf{d}_N^\alpha + (\tilde{\mathbf{g}}_{\alpha \beta I}^T - \bar{\mathbf{g}}_{\alpha \beta I}^T) \mathbf{d}_M^{\alpha \beta} \right) = -\sum_{I=1}^{n_p} \delta \mathbf{d}_I \cdot \mathbf{f}_I \quad (48)$$

269 where \mathbf{f}_I 's are the components of the traditional force vector:

$$\mathbf{f}_I = \int_{\Gamma_t} \Psi_I \bar{\mathbf{t}} d\Gamma - \int_{\Gamma_M} \Psi_{I,\gamma} n^\gamma \bar{M}_{nn} d\Gamma + [[\Psi_I \mathbf{a}_3 \bar{P}]]_{\mathbf{x} \in C_P} + \int_{\Omega} \Psi_I \bar{\mathbf{b}} d\Omega \quad (49)$$

270 The left side of Eq. (48) can be simplified using the following steps. For clarity,
 271 the derivation of first term in Eq. (48) taken as an example is given by:

$$\begin{aligned} \sum_{I=1}^{n_p} \delta \mathbf{d}_I \cdot \tilde{\mathbf{g}}_{\alpha I}^T \mathbf{d}_N^\alpha &= \sum_{I=1}^{n_p} \delta \mathbf{d}_I \cdot (\mathbf{G}^{-1} \tilde{\mathbf{g}}_{\alpha I})^T \mathbf{G} \mathbf{d}_N^\alpha \\ &= \int_{\Omega_C} \sum_{I=1}^{n_p} \delta \mathbf{d}_I \cdot (\mathbf{q}^T \mathbf{G}^{-1} \tilde{\mathbf{g}}_{\alpha I})^T \mathbf{q}^T \mathbf{d}_N^\alpha d\Omega \\ &= \int_{\Omega_C} \sum_{I=1}^{n_p} \delta \mathbf{d}_I \cdot \mathbf{a}_\beta (\mathbf{q}^T \mathbf{G}^{-1} \tilde{\mathbf{g}}_{\alpha I})^T N^{\alpha \beta h} d\Omega \\ &= \int_{\Omega_C} \delta \tilde{\varepsilon}_{\alpha \beta}^h N^{\alpha \beta h} d\Omega \end{aligned} \quad (50)$$

following the above procedure and including the weak form of Eqs. (21a), (21b),
the left side of Eq. (48) in Ω_C becomes:

$$\begin{aligned}
& \sum_{I=1}^{n_p} \delta \mathbf{d}_I \cdot \left((\tilde{\mathbf{g}}_{\alpha I}^T - \bar{\mathbf{g}}_{\alpha I}^T) \mathbf{d}_N^\alpha + (\tilde{\mathbf{g}}_{\alpha \beta I}^T - \bar{\mathbf{g}}_{\alpha \beta I}^T) \mathbf{d}_M^{\alpha \beta} \right) \\
&= \int_{\Omega_C} ((\delta \tilde{\varepsilon}_{\alpha \beta}^h - \delta \bar{\varepsilon}_{\alpha \beta}^h) N^{\alpha \beta h} + (\delta \tilde{\kappa}_{\alpha \beta}^h - \delta \bar{\kappa}_{\alpha \beta}^h) M^{\alpha \beta h}) d\Omega \\
&= \int_{\Omega_C} (\delta \tilde{\varepsilon}_{\alpha \beta}^h - \delta \bar{\varepsilon}_{\alpha \beta}^h) h C^{\alpha \beta \gamma \eta} \varepsilon_{\gamma \eta}^h + (\delta \tilde{\kappa}_{\alpha \beta}^h - \delta \bar{\kappa}_{\alpha \beta}^h) \frac{h^3}{12} C^{\alpha \beta \gamma \eta} \kappa_{\gamma \eta}^h \\
&= \int_{\Omega_C} \delta \tilde{\varepsilon}_{\alpha \beta}^h h C^{\alpha \beta \gamma \eta} \varepsilon_{\gamma \eta}^h d\Omega + \int_{\Omega_C} \delta \tilde{\kappa}_{\alpha \beta}^h \frac{h^3}{12} C^{\alpha \beta \gamma \eta} \kappa_{\gamma \eta}^h d\Omega \\
&\quad - \int_{\Omega_C} \delta \bar{\varepsilon}_{\alpha \beta}^h h C^{\alpha \beta \gamma \eta} \varepsilon_{\gamma \eta}^h d\Omega - \int_{\Omega_C} \delta \bar{\kappa}_{\alpha \beta}^h h C^{\alpha \beta \gamma \eta} \kappa_{\gamma \eta}^h d\Omega \\
&\quad - \int_{\Omega_C} \delta \tilde{\kappa}_{\alpha \beta}^h \frac{h^3}{12} C^{\alpha \beta \gamma \eta} \bar{\kappa}_{\gamma \eta}^h d\Omega - \int_{\Omega_C} \delta \bar{\kappa}_{\alpha \beta}^h \frac{h^3}{12} C^{\alpha \beta \gamma \eta} \tilde{\kappa}_{\gamma \eta}^h d\Omega \\
&\quad + \int_{\Omega_C} \delta \bar{\varepsilon}_{\alpha \beta}^h h C^{\alpha \beta \gamma \eta} \varepsilon_{\gamma \eta}^h d\Omega + \int_{\Omega_C} \delta \bar{\kappa}_{\alpha \beta}^h \frac{h^3}{12} C^{\alpha \beta \gamma \eta} \bar{\kappa}_{\gamma \eta}^h d\Omega \\
&\quad + \int_{\Omega_C} (\delta \tilde{\varepsilon}_{\alpha \beta}^h - \delta \bar{\varepsilon}_{\alpha \beta}^h) h C^{\alpha \beta \gamma \eta} \varepsilon_{\gamma \eta}^h d\Omega + \int_{\Omega_C} (\delta \tilde{\kappa}_{\alpha \beta}^h - \delta \bar{\kappa}_{\alpha \beta}^h) \frac{h^3}{12} C^{\alpha \beta \gamma \eta} \hat{\kappa}_{\gamma \eta}^h d\Omega
\end{aligned} \tag{51}$$

on further substituting Eqs. (44) and (46) into above equation gives the final
discrete equilibrium equations, respectively:

$$(\mathbf{K} + \tilde{\mathbf{K}} + \bar{\mathbf{K}}) \mathbf{d} = \mathbf{f} + \tilde{\mathbf{f}} + \bar{\mathbf{f}} \tag{52}$$

where

$$\mathbf{K}_{IJ} = \int_{\Omega} \tilde{\varepsilon}_{\alpha \beta I} h C^{\alpha \beta \gamma \eta} \tilde{\varepsilon}_{\gamma \eta J} d\Omega + \int_{\Omega} \tilde{\kappa}_{\alpha \beta I} \frac{h^3}{12} C^{\alpha \beta \gamma \eta} \tilde{\kappa}_{\alpha \beta J} d\Omega \tag{53}$$

277

$$\begin{aligned}
\tilde{\mathbf{K}}_{IJ} &= - \int_{\Gamma_v} (\Psi_I \tilde{\mathbf{T}}_{NJ} + \tilde{\mathbf{T}}_{NJ} \Psi_J) d\Gamma \\
&\quad + \int_{\Gamma_\theta} (\Psi_{I,\gamma} n^\gamma \mathbf{a}_3 \tilde{\mathbf{M}}_{nnJ} + \mathbf{a}_3 \tilde{\mathbf{M}}_{nnI} \Psi_{J,\gamma} n^\gamma) d\Gamma
\end{aligned} \tag{54a}$$

$$\begin{aligned}
&\quad + ([[\Psi_I \mathbf{a}_3 \tilde{\mathbf{P}}_J]] + [[\tilde{\mathbf{P}}_I \mathbf{a}_3 \Psi_J]])_{\mathbf{x} \in C_v} \\
\tilde{\mathbf{f}}_I &= - \int_{\Gamma_v} \tilde{\mathbf{T}}_{NI} \cdot \bar{\mathbf{v}} d\Gamma + \int_{\Gamma_\theta} \tilde{\mathbf{M}}_{nnI} \bar{\theta}_n d\Gamma + [[\tilde{\mathbf{P}}_I \mathbf{a}_3 \cdot \bar{\mathbf{v}}]]_{\mathbf{x} \in C_v}
\end{aligned} \tag{54b}$$

278

$$\bar{\mathbf{K}}_{IJ} = - \int_{\Gamma_v} \bar{\mathbf{T}}_{MI} \Psi_J d\Gamma + \int_{\Gamma_\theta} \mathbf{a}_3 \bar{\mathbf{M}}_{nnI} \Psi_{J,\gamma} n^\gamma d\Gamma + [[\bar{\mathbf{P}}_I \mathbf{a}_3 \Psi_J]]_{\mathbf{x} \in C_v} \tag{55a}$$

$$\bar{\mathbf{f}}_I = - \int_{\Gamma_v} \bar{\mathbf{T}}_{MI} \cdot \bar{\mathbf{v}} d\Gamma + \int_{\Gamma_\theta} \bar{\mathbf{M}}_{nnI} \bar{\theta}_n d\Gamma + [[\bar{\mathbf{P}}_I \mathbf{a}_3 \cdot \bar{\mathbf{v}}]]_{\mathbf{x} \in C_v} \tag{55b}$$

279 The detailed derivations of Eqs (53)-(55) are listed in the Appendix B. As
 280 shown in these equations, Eq. (53) is the conventional stiffness matrix evaluated
 281 by smoothed gradients $\tilde{\Psi}_{I,\alpha}$, $\tilde{\Psi}_{I,\alpha|\beta}$, and the Eqs. (54) and (55) contribute for
 282 the enforcement of essential boundary. It should be mentioned that, in accor-
 283 dance with reproducing kernel smoothed gradient framework, the integration
 284 scheme of Eqs. (53-55) should be aligned with the those used in the construc-
 285 tion of smoothed gradients. The integration scheme used for proposed method
 286 is shown in Fig. 2, in which the total number of the blue circular integration
 287 points has been optimized from a global point of view, aiming to reduce the com-
 288 putation of traditional meshfree shape functions and its first order derivatives.
 289 In contrast, for assembly stiffness matrix \mathbf{K} , the low order Gauss integration
 290 rule is suitable to ensure the accuracy due to the inherently variational consis-
 291 tency in smoothed gradients. The detailed positions and weight of integration
 292 points and the efficiency demonstration of this optimized integration scheme
 293 can be found in [26, 32] With a close look at Eqs. (54) and (55), the proposed
 294 approach for enforcing essential boundary conditions show an identical struc-
 295 ture with traditional Nitsche's method, both have the consistent and stabilized
 296 terms. So, the next subsection will review the Nitsche's method and compare
 297 it with the proposed method.

298 4.2. Comparison with Nitsche's method

299 The Nitsche's method for enforcing essential boundaries can be regarded as a
 300 combination of Lagrangian multiplier method and penalty method, in which the
 301 Lagrangian multiplier is represented by the approximated displacement. The
 302 corresponding total potential energy functional Π_P is given by:

$$\begin{aligned}
 \Pi_P(\mathbf{v}) = & \int_{\Omega} \frac{1}{2} \varepsilon_{\alpha\beta} N^{\alpha\beta} d\Omega + \int_{\Omega} \frac{1}{2} \kappa_{\alpha\beta} M^{\alpha\beta} d\Omega \\
 & - \int_{\Gamma_t} \mathbf{v} \cdot \bar{\mathbf{t}} d\Gamma + \int_{\Gamma_M} \mathbf{v}_{,\gamma} n^{\gamma} \mathbf{a}_3 M_{nn} d\Gamma + (\mathbf{v} \cdot \mathbf{a}_3 P)_{\mathbf{x} \in C_P} - \int_{\Omega} \mathbf{v} \cdot \bar{\mathbf{b}} d\Omega \\
 & - \underbrace{\int_{\Gamma_v} \mathbf{t} \cdot (\mathbf{v} - \bar{\mathbf{v}}) d\Gamma + \int_{\Gamma_{\theta}} M_{nn} (\theta_n - \bar{\theta}_n) d\Gamma + (P \mathbf{a}_3 \cdot (\mathbf{v} - \bar{\mathbf{v}}))_{\mathbf{x} \in C_v}}_{\text{consistent term}} \quad (56) \\
 & + \underbrace{\sum_{i=1}^3 \frac{\alpha_{vi}}{2} \int_{\Gamma_v} \mathbf{v} \cdot \mathbf{v} d\Gamma + \frac{\alpha_{\theta}}{2} \int_{\Gamma_{\theta}} \theta_n^2 d\Gamma + \frac{\alpha_C}{2} (\mathbf{v} \cdot \mathbf{a}_3)_{\mathbf{x} \in C_v}^2}_{\text{stabilized term}}
 \end{aligned}$$

303 where the consistent term generated from the Lagrangian multiplier method
 304 contributes to enforce the essential boundary, and meet the variational con-
 305 sistency condition. However, the consistent term can not always ensure the
 306 coercivity of stiffness, so the penalty method is introduced to serve as a sta-
 307 bilized term, in which α_{vi} 's, α_{θ} and α_C are experimental artificial parameters
 308 in penalty method. With a standard variational argument, the corresponding

309 weak form can be stated as:

$$\begin{aligned}
\delta \Pi_P(\mathbf{v}) &= \int_{\Omega} \delta \varepsilon_{\alpha\beta} N^{\alpha\beta} d\Omega + \int_{\Omega} \delta \kappa_{\alpha\beta} M^{\alpha\beta} d\Omega \\
&\quad - \int_{\Gamma_t} \delta \mathbf{v} \cdot \bar{\mathbf{t}} d\Gamma + \int_{\Gamma_M} \delta \mathbf{v}_{,\gamma} n^{\gamma} \mathbf{a}_3 M_{nn} d\Gamma + (\delta \mathbf{v} \cdot \mathbf{a}_3 P)_{\mathbf{x} \in C_P} - \int_{\Omega} \delta \mathbf{v} \cdot \bar{\mathbf{b}} d\Omega \\
&\quad - \int_{\Gamma_v} \delta \mathbf{v} \cdot \mathbf{t} d\Gamma + \int_{\Gamma_{\theta}} \delta \theta_{\mathbf{n}} M_{nn} d\Gamma + (\mathbf{v} \cdot \mathbf{a}_3 P)_{\mathbf{x} \in C_v} \\
&\quad - \int_{\Gamma_v} \delta \mathbf{t} \cdot (\mathbf{v} - \bar{\mathbf{v}}) d\Gamma + \int_{\Gamma_{\theta}} \delta M_{nn} (\theta_{\mathbf{n}} - \bar{\theta}_{\mathbf{n}}) d\Gamma + (\delta P \mathbf{a}_3 \cdot (\mathbf{v} - \bar{\mathbf{v}}))_{\mathbf{x} \in C_v} \\
&\quad + \sum_{i=1}^3 \alpha_{vi} \int_{\Gamma_v} (\delta \mathbf{v} \cdot \mathbf{a}_i) (\mathbf{a}_i \cdot \mathbf{v}) d\Gamma + \alpha_{\theta} \int_{\Gamma_{\theta}} \delta \theta_{\mathbf{n}} \theta_{\mathbf{n}} d\Gamma + \alpha_C (\delta \mathbf{v} \cdot \mathbf{a}_3 \mathbf{a}_3 \cdot \mathbf{v})_{\mathbf{x} \in C_v} \\
&= 0
\end{aligned} \tag{57}$$

310 Further invoking the conventional reproducing kernel approximation of Eq. (22)
311 leads to the following discrete equilibrium equations:

$$\sum_{J=1}^{n_p} (\mathbf{K}_{IJ} + \mathbf{K}_{IJ}^c + \mathbf{K}_{IJ}^s) \mathbf{d}_J = \mathbf{f}_I + \mathbf{f}^c + \mathbf{f}^s \tag{58}$$

312 where the stiffness \mathbf{K}_{IJ} is identical with Eq. (53). \mathbf{K}_{IJ}^c and \mathbf{K}_{IJ}^s are the stiffness
313 matrices for consistent and stabilized terms, respectively, and have the following
314 form:

$$\begin{aligned}
\mathbf{K}_{IJ}^c &= - \int_{\Gamma_v} (\Psi_I \mathbf{T}_{NJ} + \mathbf{T}_{NJ} \Psi_J) d\Gamma \\
&\quad + \int_{\Gamma_{\theta}} (\Psi_{I,\gamma} n^{\gamma} \mathbf{a}_3 M_{nnJ} + \mathbf{a}_3 M_{nnI} \Psi_{I,\gamma} n^{\gamma}) d\Gamma \\
&\quad + ([\Psi_I \mathbf{a}_3 \mathbf{P}_J] + [\mathbf{P}_I \mathbf{a}_3 \Psi_J])_{\mathbf{x} \in C_v}
\end{aligned} \tag{59a}$$

$$\mathbf{f}_I^c = - \int_{\Gamma_v} \mathbf{T}_I \cdot \bar{\mathbf{v}} d\Gamma + \int_{\Gamma_{\theta}} M_{nnI} \bar{\theta}_{\mathbf{n}} d\Gamma + [\mathbf{P}_I \mathbf{a}_3 \cdot \bar{\mathbf{v}}]_{\mathbf{x} \in C_v} \tag{59b}$$

315

$$\mathbf{K}_{IJ}^s = \alpha_v \int_{\Gamma_v} \Psi_I \Psi_J d\Gamma + \alpha_{\theta} \int_{\Gamma_{\theta}} \Psi_{I,\eta} n^{\eta} \mathbf{a}_3 \mathbf{a}_3 n^{\gamma} \Psi_{J,\gamma} d\Gamma + \alpha_C [\Psi_I \mathbf{a}_3 \mathbf{a}_3 \Psi_J]_{\mathbf{x} \in C_v} \tag{60a}$$

$$\mathbf{f}_I^s = \alpha_v \int_{\Gamma_v} \Psi_I \bar{\mathbf{v}} d\Gamma + \alpha_{\theta} \int_{\Gamma_{\theta}} \Psi_{I,\eta} n^{\eta} \mathbf{a}_3 \bar{\theta}_{\mathbf{n}} d\Gamma + \alpha_C [\Psi_I \mathbf{a}_3 \mathbf{a}_3 \cdot \bar{\mathbf{v}}]_{\mathbf{x} \in C_v} \tag{60b}$$

316 with

$$\boldsymbol{\alpha}_v = \begin{bmatrix} \alpha_{v1} & 0 & 0 \\ 0 & \alpha_{v2} & 0 \\ 0 & 0 & \alpha_{v3} \end{bmatrix} \tag{61}$$

317 On comparing with the consistent terms of Eqs. (54) and (59), the expres-
 318 sions were almost identical, the major difference is that the higher order deriva-
 319 tives of shape functions have been replaced by smoothed gradients. Owing to
 320 the reproducing kernel framework, the construction of smoothed gradients only
 321 concerned about the computation of traditional meshfree shape functions and
 322 their first order derivatives, which avoid the costly computation of higher order
 323 derivatives. Moreover, the stabilized terms in Eq. (60) employs the penalty
 324 method with big enough artificial parameters to ensure the coercivity of stiff-
 325 ness. And the optimal values of these artificial parameters are proportional to
 326 the grid size of discrete model that can be represented by support size in mesh-
 327 free approximation, where the $\alpha_{v\alpha} \propto s^{-1}$, $\alpha_{v3} \propto s^{-3}$, $\alpha_{\theta} \propto s^{-1}$, $\alpha_C \propto s^{-2}$ [30],
 328 and $s = \min\{s_{\alpha I}\}$. In contrast, the stabilized term of Eq. (55) naturally exists
 329 in its weak form, and can stabilize the result without considering any artificial
 330 parameters.

331 5. Numerical examples

332 The suggested method, which uses Nitsche's method, the consistent repro-
 333 ducing kernel gradient smoothing integration scheme (RKGSI), and the non-
 334 consistent Gauss integration scheme (GI) with penalty method, as well as the
 335 proposed Hu-Washizu formulation (HW) to enforce the necessary boundary con-
 336 ditions, is validated in this section through several examples. A normalized
 337 support size of 2.5 is used for all the methods to ensure the requirement of
 338 quadratic base meshfree approximation. To eliminate the influence of integra-
 339 tion, the Gauss integration scheme uses 6 Gauss points for domain integration
 340 and 3 points for boundary integration, so as to maintain the same integration
 341 accuracy between domain and boundaries. Moreover, the number of integra-
 342 tion points are identical between the Gauss and RKGSI schemes. The error
 343 estimates of displacement (L_2 -Error) and energy (H_e -Error) is used here:

$$\begin{aligned}
 L_2\text{-Error} &= \frac{\sqrt{\int_{\Omega} (\mathbf{v} - \mathbf{v}^h) \cdot (\mathbf{v} - \mathbf{v}^h) d\Omega}}{\sqrt{\mathbf{v} \cdot \mathbf{v}}} \\
 H_e\text{-Error} &= \frac{\sqrt{\int_{\Omega} \left((\varepsilon_{\alpha\beta} - \varepsilon_{\alpha\beta}^h)(N^{\alpha\beta} - N^{\alpha\beta h}) + \int_{\Omega} (\kappa_{\alpha\beta} - \kappa_{\alpha\beta}^h)(M^{\alpha\beta} - M^{\alpha\beta h}) \right) d\Omega}}{\sqrt{\int_{\Omega} (\varepsilon_{\alpha\beta} N^{\alpha\beta} + \kappa_{\alpha\beta} M^{\alpha\beta}) d\Omega}}
 \end{aligned}
 \tag{62}$$

344 5.1. Patch tests

345 The linear and quadratic patch tests for flat and curved thin shells are firstly
 346 studied to verify the variational consistency of the proposed method. As shown
 347 in Fig. 3, the flat and curved models are depicted by an identical parametric
 348 domain $\Omega = (0, 1) \otimes (0, 1)$, where the cylindrical coordinate system with radius
 349 $R = 1$ is employed to describe the curved model, and the whole domain Ω
 350 is discretized by the 165 meshfree nodes. The artificial parameters of $\alpha_v =$
 351 10^5 , $\alpha_{\theta} = 10^3$, $\alpha_C = 10^5$ and $\alpha_v = 10^9$, $\alpha_{\theta} = 10^9$, $\alpha_C = 10^9$ are used for Nitsche's
 352 method and penalty method respectively. All the boundaries are enforced as
 353 essential boundary conditions with the following manufactured exact solution:

$$\mathbf{v} = \begin{Bmatrix} (\xi^1 + 2\xi^2)^n \\ (3\xi^1 + 4\xi^2)^n \\ (5\xi^1 + 6\xi^2)^n \end{Bmatrix}, \quad n = \begin{cases} 1 & \text{Linear patch test} \\ 2 & \text{Quadratic patch test} \end{cases}
 \tag{63}$$

354 Table 1 lists the L_2 - and H_e -Error results of patch test with flat model, where
 355 the RKGSI scheme with variational consistent essential boundary enforcement,
 356 i.e. RKGSI-Nitsche and RKGSI-HW, can pass the linear and quadratic patch
 357 test. In contrast, the RKGSI-Penalty cannot pass the patch test since the
 358 Penalty method is unable to ensure the variational consistency. Due to the
 359 loss of variational consistency condition, even with Nitsche's method, Gauss
 360 meshfree formulations show noticeable errors. Table 2 shows the results for
 361 curved model, which indicated that all the considered methods cannot pass the

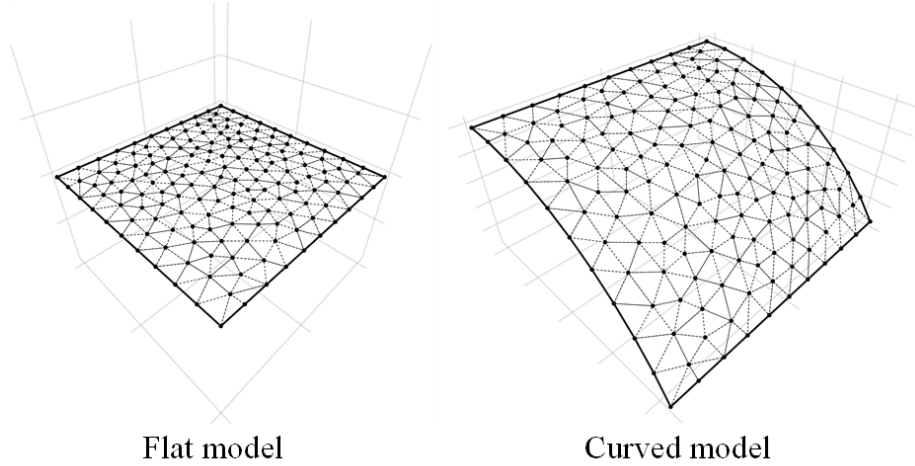


Figure 3: Meshfree discretization for patch test

patch test. This is mainly because the proposed smoothed gradient of Eqs. (35) and (36) could not exactly reproduce the non-polynomial membrane and bending stress. However, the RKGSI-HW and RKGSI-Nitsche methods also provide better accuracy compared to others due to the fulfillment of first second-order variational consistency. And, even only with local variational consistency, the RKGSI-Penalty obtained a better result than traditional Gauss scheme. Meanwhile, the bending moment contours of M^{12} are listed in Fig. 4, which further verify that the proposed method provided a satisfactory result compared to exact solution. On the other hand, the RKGSI-Penalty and the conventional Gauss meshree formulations showed errors.

Table 1: Results of patch test for flat model.

	Linear patch test		Quadratic patch test	
	L_2 -Error	H_e -Error	L_2 -Error	H_e -Error
GI-Penalty	$4.45E-4$	$1.35E-2$	$2.01E-3$	$1.63E-2$
GI-Nitsche	$4.51E-4$	$1.42E-2$	$1.22E-3$	$1.68E-2$
RKGSI-Penalty	$3.64E-9$	$6.77E-8$	$4.54E-9$	$6.57E-8$
RKGSI-Nitsche	$3.31E-12$	$1.34E-11$	$5.98E-12$	$1.21E-11$
RKGSI-HR	$6.67E-13$	$1.50E-11$	$1.07E-12$	$1.26E-11$

5.2. Scordelis-Lo roof

This example considers the classical Scordelis-Lo roof problem, as depicted in Fig. 5. The cylindrical roof has dimensions $R = 25$, $L = 50$, $h = 0.25$, Young's modulus $E = 4.32 \times 10^8$ and Poisson's ratio $\nu = 0.0$. The entire roof

Table 2: Results of patch test for cylindrical model.

	Linear patch test		Quadratic patch test	
	L_2 -Error	H_e -Error	L_2 -Error	H_e -Error
GI-Penalty	$3.79E-4$	$1.30E-2$	$1.74E-3$	$1.37E-2$
GI-Nitsche	$4.04E-4$	$1.42E-2$	$1.15E-3$	$1.49E-2$
RKGSi-Penalty	$1.47E-4$	$5.39E-3$	$2.26E-4$	$2.09E-3$
RKGSi-Nitsche	$2.41E-6$	$7.37E-5$	$2.47E-6$	$2.89E-5$
RKGSi-HR	$4.28E-6$	$1.30E-4$	$9.69E-6$	$2.41E-4$

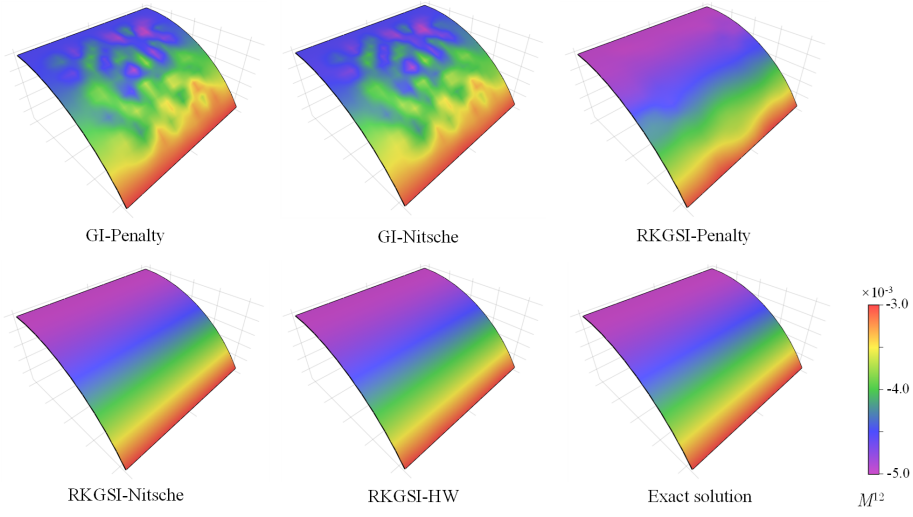


Figure 4: Contour plots of M^{12} for curved shell patch test.

is subjected to an uniform body force of $b_z = -90$, with the straight edges remaining free and the the curved edges are enforced by $v_x = v_z = 0$.

Due to the symmetry, only a quadrant of the model is considered for meshfree analysis, which is discretized by the 11×16 , 13×20 , 17×24 and 19×28 meshfree nodes, as listed in Fig. 6. The comparison of the displacement in z -direction at node A , v_{A3} , is used as the investigated quantity, with the reference value 0.3006 given by [33]. Firstly, Fig. 7 presents a sensitivity study for the artificial parameters of α_{vi} 's and α_θ 's in the RKGSi meshfree formulations with Nitsche's method and penalty method, where all of the parameters are scaled by the support size as, $\alpha_{v\alpha} = s^{-1}\bar{\alpha}_v$, $\alpha_{v3} = s^{-3}\bar{\alpha}_v$ and $\alpha_\theta = s^{-1}\bar{\alpha}_\theta$. For a better comparison, the result of proposed RKGSi-HW is also listed in this figure. The results of Fig. 7 revealed, Nitsche's method observed less artificial sensitivity. However, both the methods cannot trivially determine the optimal values of the artificial parameters. The optimal artificial parameters from Fig. 7 are adopted for the convergence study in Fig. 8. The convergence result showed

391 that the RKGSi get satisfactory results while the traditional Gauss methods
 392 demonstrated noticeable errors.

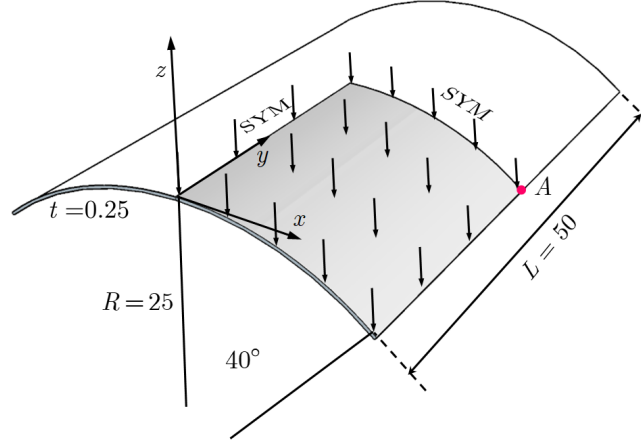


Figure 5: Description of Scordelis-Lo roof problem.

393 5.3. Pinched Hemispherical shell

394 Consider the hemispherical shell shown in Fig. 9, which is loaded at four
 395 points $P = \pm 2$ at 90° interval at its bottom. The hemispherical shell has an
 396 radius $R = 10$, thickness $h = 0.04$, Young's modulus $E = 6.825 \times 10^7$ and
 397 Poisson's ratio $\nu = 0.3$.

398 Due to symmetry, only quadrant model, where the 16×16 , 24×24 , 32×32
 399 and 40×40 meshfree nodes have been discretized as shown in Fig. (10), was con-
 400 sidered. The quantity under investigation for convergence is the displacement
 401 at x -direction on point A, v_{A1} . Fig. 11 displays the corresponding convergence
 402 results, indicating the RKGSi scheme performed significantly better compared
 403 to the GI meshfree formulation. Meanwhile, the efficiency comparison for this
 404 problem is also shown in Fig. 12, in which the CPU time for assembly and
 405 calculation of shape functions are considered. Fig. 12(a) indicates that the
 406 RKGSi scheme observed high efficiency in assembly. This is due to the vari-
 407 ational inconsistent Gauss meshfree formulation which require more Gaussian
 408 points to get satisfactory results. Fig. 12(b) lists the CPU time spent on enforc-
 409 ing essential boundary conditions for the penalty method, Nitsche's method and
 410 proposed HW method. The results highlighted that the proposed HW method
 411 consumed comparable CPU time in assembly compared to Nitsche's method.
 412 However, less time was spent to calculate the shape functions. Since both the
 413 HW method and penalty method were developed considering the shape func-
 414 tions first order derivatives. For this reason, both the methods shared an almost
 415 identical time in computing the shape functions.

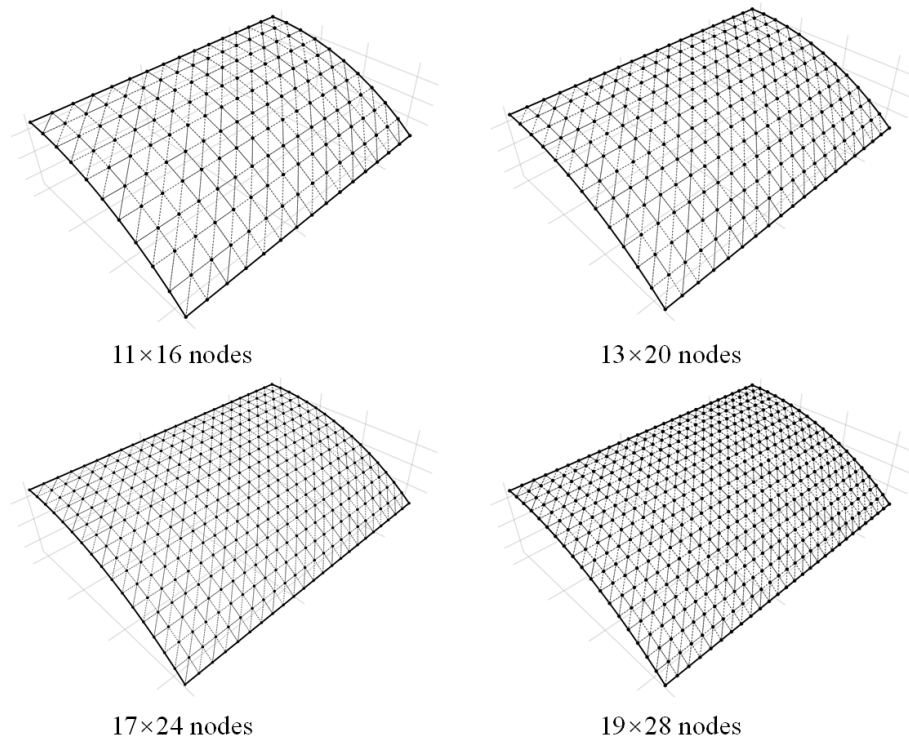


Figure 6: Meshfree discretizations for Scordelis-Lo roof problem.

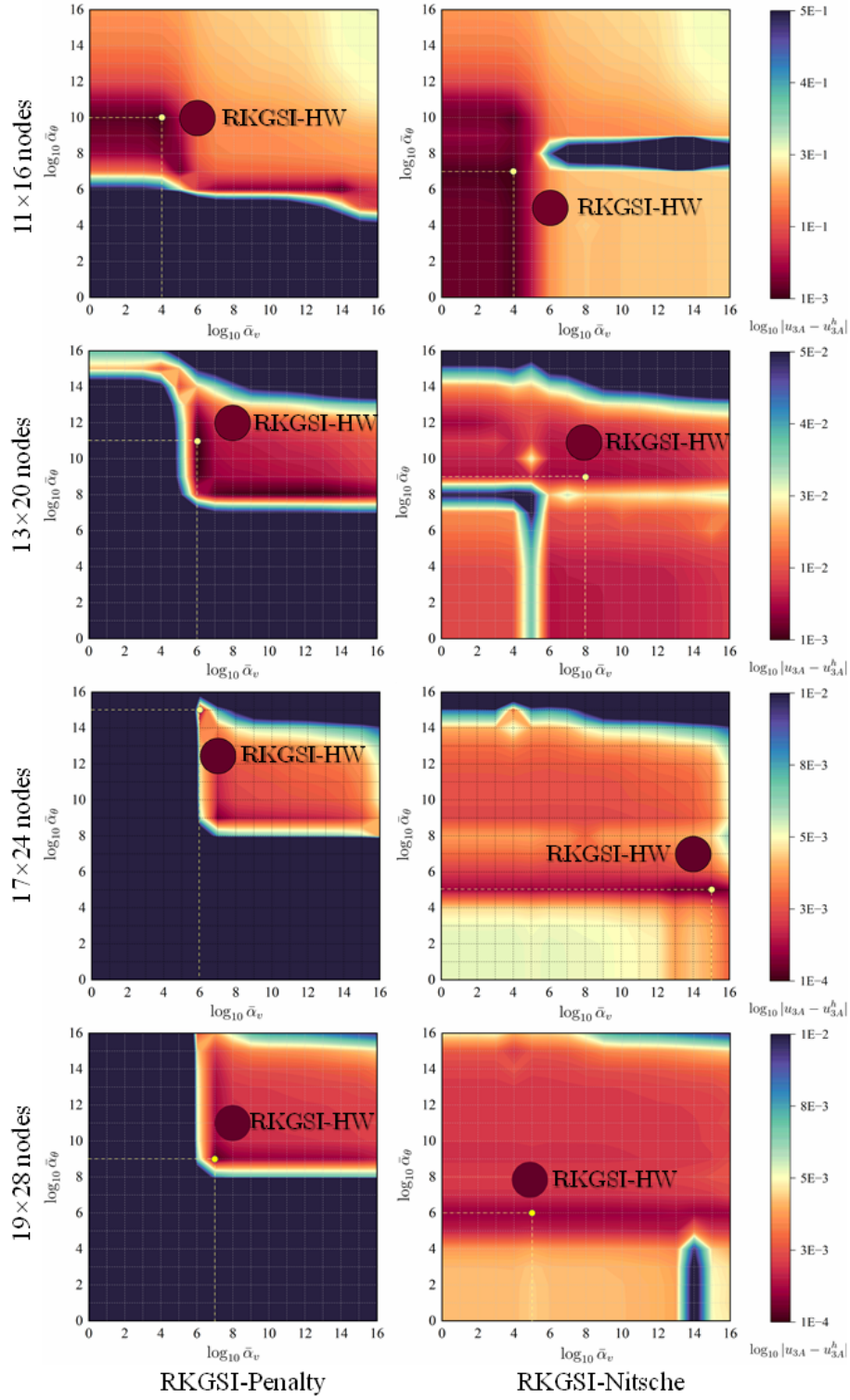


Figure 7: Sensitivity comparison of α_v and α_θ for Scordelis-Lo problem.

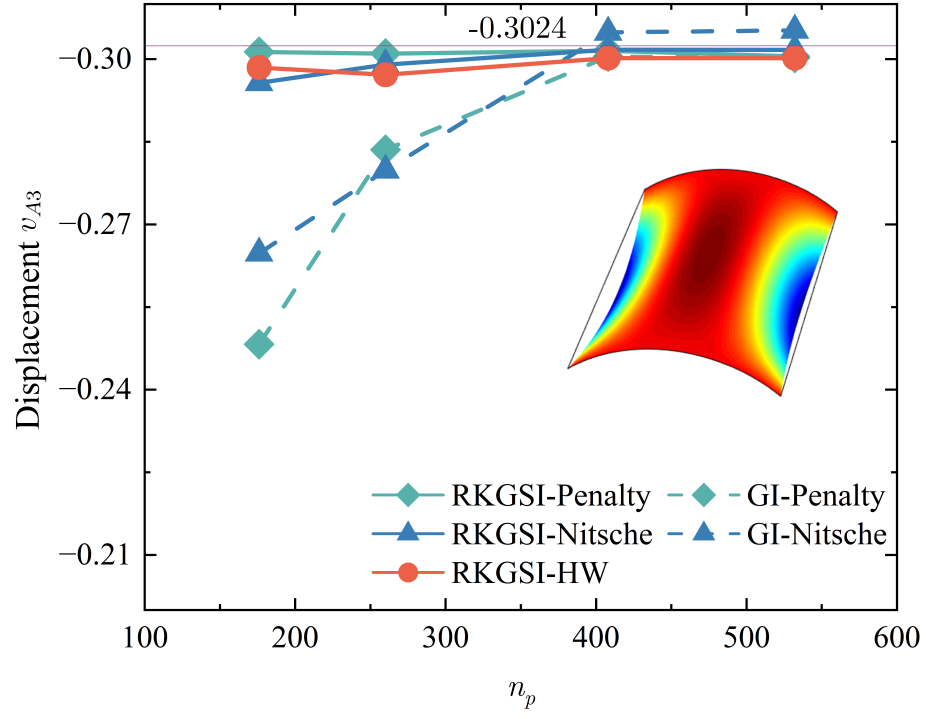


Figure 8: Displacement convergence for Scordelis-Lo roof problem.

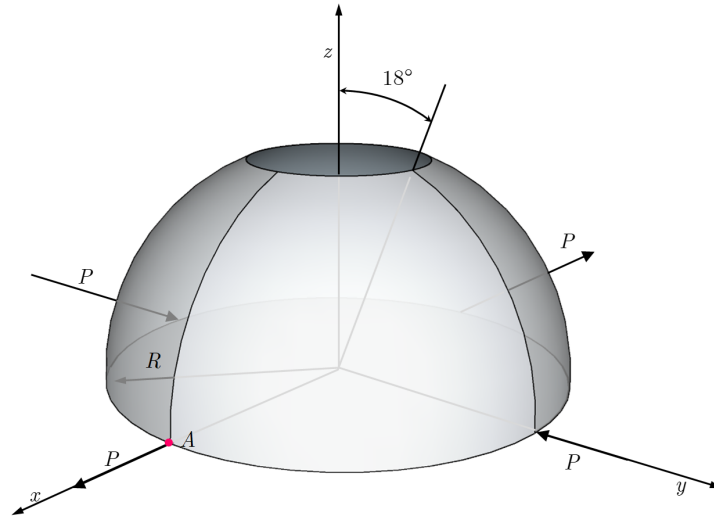
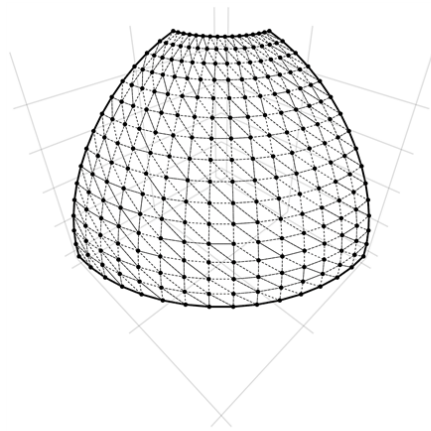
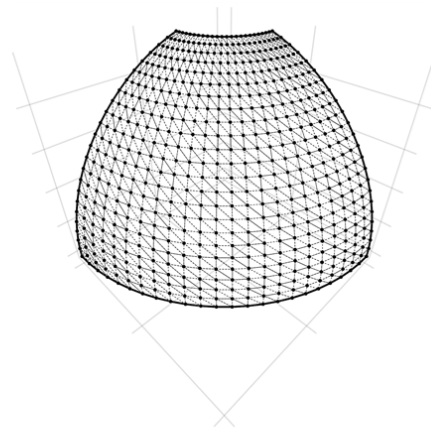


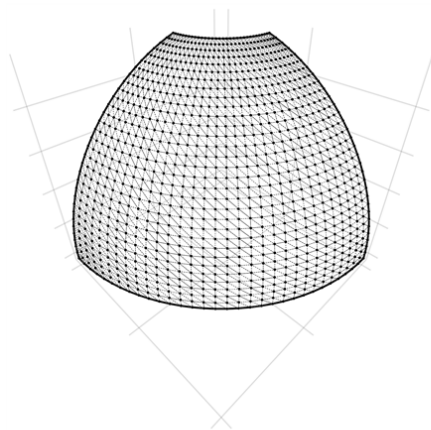
Figure 9: Description of pinched hemispherical shell problem.



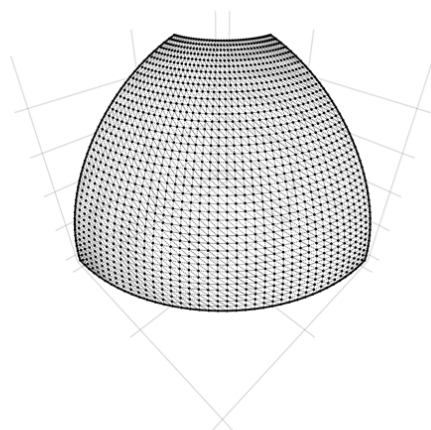
16×16 nodes



24×24 nodes



32×32 nodes



40×40 nodes

Figure 10: Meshfree discretizations for pinched hemispherical shell problem.

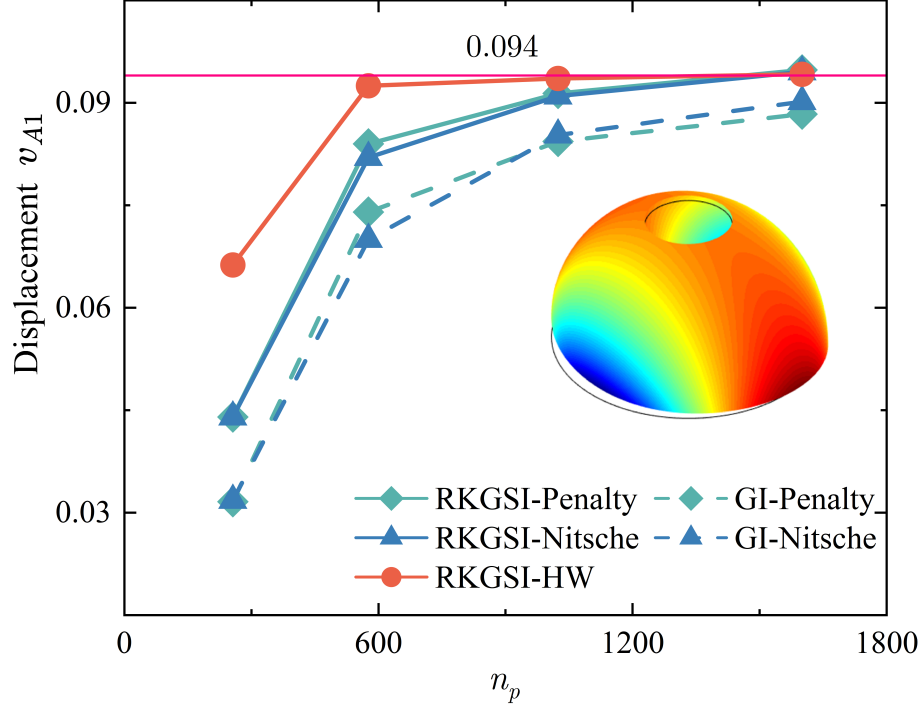


Figure 11: Displacement convergence for pinched hemispherical shell problem.

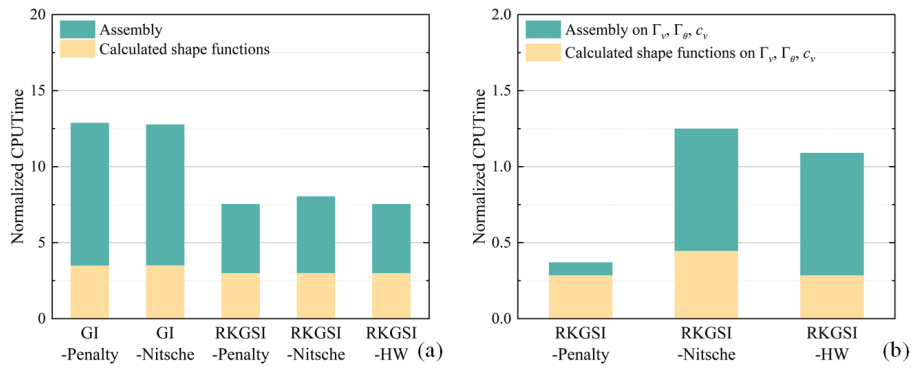


Figure 12: efficiency comparison for pinched hemispherical shell problem: (a) Whole domain; (b) Essential boundaries

416 6. Conclusion

417 In this study, an efficient and quasi-consistent meshfree thin shell formu-
418 lation was presented to naturally enforce the essential boundary conditions.
419 Mixed formulation with the Hu-Washizu principle weak form is adopted, where
420 the traditional meshfree shape functions discretized the displacement, and the
421 strains and stresses were expressed by the reproducing kernel smoothed gradi-
422 ents and the covariant smoothed gradients, respectively. The smoothed gradi-
423 ent naturally embedded the first second-order integration constraints and has
424 a quasi variational consistency for the curved models in each integration cell.
425 Owing to the Hu-Washizu variational principle, the essential boundary condi-
426 tion enforcement has a similar form with the conventional Nitsche's method;
427 both have consistent and stabilized terms. The costly high order derivatives in
428 the Nitsche's consistent term have been replaced by the smoothed gradients,
429 which improved the computational speed due to the reproducing kernel gradi-
430 ent smoothing framework. Furthermore, the stabilized term naturally existed
431 in the Hu-Washizu weak form, and the artificial parameter needed in Nitsche's
432 stabilized term has vanished, which can automatically maintain the coercivity
433 for the stiffness matrix. Based on general reproducing kernel gradient smooth-
434 ing framework, the proposed methodology can be trivially extended to high
435 order basis meshfree formulation. The numerical results demonstrated that the
436 proposed Hu-Washizu quasi-consistent meshfree thin shell formulation showed
437 excellent accuracy, efficiency, and stability.

Acknowledgment

The support of this work by the National Natural Science Foundation of China (12102138, 52350410467) and the Natural Science Foundation of Fujian Province of China (2023J01108, 2022J05056) is gratefully acknowledged.

442 Appendix A. Green's theorems for in-plane vector

443 This Appendix discusses two kinds of Green's theorems used for the devel-
 444 opment of the proposed meshfree method. For an arbitrary vectors v^α and a
 445 scalar function f , with Green's theorem for in-plane vector, the first Green's
 446 theorem is listed as follows [30]:

$$\begin{aligned} \int_{\Omega} f_{,\alpha} v^\alpha d\Omega &= \int_{\Gamma} f v^\alpha n_\alpha d\Gamma - \int_{\Omega} f (v_{,\alpha}^\alpha + \Gamma_{\beta\alpha}^\beta v^\alpha) d\Omega \\ &= \int_{\Gamma} f v^\alpha n_\alpha d\Gamma - \int_{\Omega} f v^\alpha|_\alpha d\Omega \end{aligned} \quad (\text{A.1})$$

447 where $\Gamma_{\alpha\beta}^\gamma = \mathbf{a}_{\alpha,\beta} \cdot \mathbf{a}^\gamma$ denotes the Christoffel symbol of the second kind. $v^\alpha|_\alpha$
 448 can be represented as the in-plane covariant derivative of the vector v^α :

$$v^\alpha|_\alpha = v_{,\alpha}^\alpha + \Gamma_{\beta\alpha}^\beta v^\alpha \quad (\text{A.2})$$

449 The second Green's theorem is established with a mixed form of second
 450 order derivative. Let $A^{\alpha\beta}$ can be an arbitrary symmetric second order tensor,
 451 the Green's theorem yields [30]:

$$\begin{aligned} \int_{\Omega} f_{,\alpha}|_\beta A^{\alpha\beta} d\Omega &= \int_{\Gamma} f_{,\gamma} n^\gamma A^{\alpha\beta} n_\alpha n_\beta d\Gamma - \int_{\Gamma} f (A^{\alpha\beta} s_\alpha n_\beta)_{,\gamma} s^\gamma d\Gamma + [[f A^{\alpha\beta} s_\alpha n_\beta]]_{\mathbf{x} \in C} \\ &\quad - \int_{\Gamma} f (A_{,\beta}^{\alpha\beta} n_\alpha + \Gamma_{\alpha\beta}^\gamma A^{\alpha\beta} n_\gamma + \Gamma_{\gamma\beta}^\gamma A^{\alpha\beta} n_\alpha) d\Gamma \\ &\quad + \int_{\Omega} f \left(\Gamma_{\alpha\beta,\gamma}^\gamma A^{\alpha\beta} + \Gamma_{\alpha\beta}^\gamma A_{,\gamma}^{\alpha\beta} + \Gamma_{\eta\gamma}^\eta \Gamma_{\alpha\beta}^\gamma A^{\alpha\beta} \right. \\ &\quad \left. + A_{,\alpha\beta}^{\alpha\beta} + \Gamma_{\gamma\beta,\alpha}^\gamma A^{\alpha\beta} + 2\Gamma_{\gamma\alpha}^\gamma A_{,\beta}^{\alpha\beta} + \Gamma_{\gamma\alpha}^\gamma \Gamma_{\eta\beta}^\eta A^{\alpha\beta} \right) d\Omega \\ &= \int_{\Gamma} f_{,\gamma} n^\gamma A^{\alpha\beta} n_\alpha n_\beta d\Gamma - \int_{\Gamma} f (A^{\alpha\beta} s_\alpha n_\beta)_{,\gamma} s^\gamma d\Gamma + [[f A^{\alpha\beta} s_\alpha n_\beta]]_{\mathbf{x} \in C} \\ &\quad - \int_{\Gamma} f A^{\alpha\beta}|_\beta n_\alpha d\Gamma + \int_{\Omega} f A^{\alpha\beta}|_{\alpha\beta} d\Omega \end{aligned} \quad (\text{A.3})$$

452 with

$$A^{\alpha\beta}|_\beta = A_{,\beta}^{\alpha\beta} + \Gamma_{\beta\gamma}^\alpha A^{\beta\gamma} + \Gamma_{\gamma\beta}^\gamma A^{\alpha\beta} \quad (\text{A.4})$$

453

$$\begin{aligned} A^{\alpha\beta}|_{\alpha\beta} &= \Gamma_{\alpha\beta,\gamma}^\gamma A^{\alpha\beta} + \Gamma_{\alpha\beta}^\gamma A_{,\gamma}^{\alpha\beta} + \Gamma_{\eta\gamma}^\eta \Gamma_{\alpha\beta}^\gamma A^{\alpha\beta} \\ &\quad + A_{,\alpha\beta}^{\alpha\beta} + \Gamma_{\gamma\beta,\alpha}^\gamma A^{\alpha\beta} + 2\Gamma_{\gamma\alpha}^\gamma A_{,\beta}^{\alpha\beta} + \Gamma_{\gamma\alpha}^\gamma \Gamma_{\eta\beta}^\eta A^{\alpha\beta} \end{aligned} \quad (\text{A.5})$$

454 For the sake of brevity, the notion of covariant derivative is extended to a
 455 scalar function as:

$$f|_\alpha = f_{,\alpha} + \Gamma_{\beta\alpha}^\beta f \quad (\text{A.6})$$

456

$$f|_\beta n_\alpha = f_{,\beta} n_\alpha + \Gamma_{\alpha\beta}^\gamma f n_\gamma + \Gamma_{\gamma\beta}^\gamma f n_\alpha \quad (\text{A.7})$$

457

$$\begin{aligned} f|_{\alpha\beta} &= \Gamma_{\alpha\beta,\gamma}^\gamma f + \Gamma_{\alpha\beta}^\gamma f_{,\gamma} + \Gamma_{\eta\gamma}^\eta \Gamma_{\alpha\beta}^\gamma f \\ &\quad + f_{,\alpha\beta} + \Gamma_{\gamma\beta,\alpha}^\gamma f + 2\Gamma_{\gamma\alpha}^\gamma f_{,\beta} + \Gamma_{\gamma\alpha}^\gamma \Gamma_{\eta\beta}^\eta f \end{aligned} \quad (\text{A.8})$$

458 Appendix B. Derivations for stiffness metrics and force vectors

459 This Appendix details the derivations of stiffness matrices and force vectors
 460 in Eqs. (53)-(55), where the relationships of Eqs. (40), (41), (44) and (46) are
 461 used herein. Firstly, the membrane strain terms are considered as follows:

$$\begin{aligned}
 & \sum_{C=1}^{n_e} \int_{\Omega_C} \delta \tilde{\varepsilon}_{\alpha\beta}^h h C^{\alpha\beta\gamma\eta} \tilde{\varepsilon}_{\gamma\eta}^h d\Omega \\
 &= \sum_{C=1}^{n_e} \sum_{I,J=1}^{n_p} \delta \mathbf{d}_I \cdot \underbrace{\int_{\Omega_C} \tilde{\varepsilon}_{\alpha\beta I} h C^{\alpha\beta\gamma\eta} \mathbf{a}_\gamma \mathbf{q}^T d\Omega \mathbf{G}^{-1} \bar{\mathbf{g}}_{\eta J}}_{\tilde{\mathbf{g}}_I^{\eta T}} \cdot \mathbf{d}_J \\
 &= \sum_{C=1}^{n_e} \sum_{I,J=1}^{n_p} \delta \mathbf{d}_I \cdot \int_{\Gamma_C \cap \Gamma_v} \Psi_J \mathbf{q}^T \underbrace{\mathbf{G}^{-1} \tilde{\mathbf{g}}_I^\alpha n_\alpha}_{\tilde{\mathbf{T}}_{NI}} d\Gamma \cdot \mathbf{d}_J \\
 &= \sum_{I,J=1}^{n_p} \delta \mathbf{d}_I \cdot \int_{\Gamma_v} \tilde{\mathbf{T}}_{NI} \Psi_J d\Gamma \cdot \mathbf{d}_J
 \end{aligned} \tag{B.1}$$

462 with

$$463 \quad \tilde{\mathbf{g}}_I^\alpha = \mathbf{q} \mathbf{a}_\beta h C^{\alpha\beta\gamma\eta} \tilde{\varepsilon}_{\gamma\eta I} \tag{B.2}$$

$$464 \quad \tilde{\mathbf{T}}_{NI} = \mathbf{q}^T \mathbf{G}^{-1} \tilde{\mathbf{g}}_I^\alpha n_\alpha \tag{B.3}$$

Following this path, the bending strain terms can be reorganized by:

$$\begin{aligned}
 & \sum_{C=1}^{n_e} \int_{\Omega_C} \delta \tilde{\kappa}_{\alpha\beta}^h \frac{h^3}{12} C^{\alpha\beta\gamma\eta} \tilde{\kappa}_{\gamma\eta}^h d\Omega \\
 &= \sum_{C=1}^{n_e} \sum_{I,J=1}^{n_p} \delta \mathbf{d}_I \cdot \underbrace{\int_{\Omega_C} \tilde{\kappa}_{\alpha\beta I} \frac{h^3}{12} C^{\alpha\beta\gamma\eta} \mathbf{a}_3 \mathbf{q}^T d\Omega \mathbf{G}^{-1} \bar{\mathbf{g}}_{\gamma\eta J}}_{\tilde{\mathbf{g}}_I^{\gamma\eta T}} \cdot \mathbf{d}_J \\
 &= \sum_{C=1}^{n_e} \sum_{I,J=1}^{n_p} \delta \mathbf{d}_I \cdot \left(\begin{aligned} & \int_{\Gamma_C \cap \Gamma_\theta} \underbrace{\mathbf{q}^T \mathbf{G}^{-1} \tilde{\mathbf{g}}_I^{\alpha\beta} n_\alpha n_\beta}_{\tilde{\mathbf{M}}_{nnI}} n^\gamma \Psi_{J,\gamma} d\Gamma \\ & - \int_{\Gamma_C \cap \Gamma_v} \underbrace{(\mathbf{q}_{|\beta}^T \mathbf{G}^{-1} \tilde{\mathbf{g}}_I^{\alpha\beta} n_\alpha + (\mathbf{q}^T \mathbf{G}^{-1} \tilde{\mathbf{g}}_I^{\alpha\beta} s_\alpha n_\beta)_{,\gamma} s^\gamma)}_{\tilde{\mathbf{T}}_{MI}} \Psi_J d\Gamma \\ & + [[\underbrace{\mathbf{q}^T \mathbf{G}^{-1} \tilde{\mathbf{g}}_I^{\alpha\beta} s_\alpha n_\beta}_{\tilde{\mathbf{P}}_I \mathbf{a}_3} \Psi_J]]_{\mathbf{x} \in C_C \cap C_v} \end{aligned} \right) \cdot \mathbf{d}_J \\
 &= \sum_{I,J=1}^{n_p} \delta \mathbf{d}_I \cdot \left(\int_{\Gamma_\theta} \tilde{\mathbf{M}}_{nnI} n^\gamma \Psi_{J,\gamma} d\Gamma - \int_{\Gamma_v} \tilde{\mathbf{T}}_{MI} \Psi_J d\Gamma + [[\tilde{\mathbf{P}}_I \Psi_J]]_{\mathbf{x} \in C_v} \right)
 \end{aligned} \tag{B.4}$$

465 with

$$\tilde{\mathbf{g}}_I^{\alpha\beta} = \int_{\Omega_C} \mathbf{q} \frac{h^3}{12} C^{\alpha\beta\gamma\eta} \mathbf{a}_3 \tilde{\kappa}_{\gamma\eta I} d\Omega \quad (\text{B.5})$$

466

$$\begin{cases} \tilde{M}_{nnI} = \mathbf{q}^T \mathbf{G}^{-1} \tilde{\mathbf{g}}_I^{\alpha\beta} n_\alpha n_\beta \\ \tilde{\mathbf{T}}_{MI} = \mathbf{q}_{|\beta}^T \mathbf{G}^{-1} \tilde{\mathbf{g}}_I^{\alpha\beta} n_\alpha + (\mathbf{q}^T \mathbf{G}^{-1} \tilde{\mathbf{g}}_I^{\alpha\beta} s_\alpha n_\beta)_{,\gamma} s^\gamma \\ \tilde{\mathbf{P}}_I = \mathbf{q}^T \mathbf{G}^{-1} \tilde{\mathbf{g}}_I^{\alpha\beta} s_\alpha n_\beta \cdot \mathbf{a}_3 \end{cases} \quad (\text{B.6})$$

467 References

- 468 [1] L. H. Donnell, Beams, Plates and Shells, McGraw-Hill, 1976.
- 469 [2] T. J. Hughes, The Finite Element Method: Linear Static and Dynamic
470 Finite Element Analysis, Dover Publications, Mineola, New York, 2000.
- 471 [3] T. Belytschko, Y. Y. Lu, L. Gu, Element-free Galerkin methods, Interna-
472 tional Journal for Numerical Methods in Engineering 37 (1994) 229–256.
- 473 [4] W. K. Liu, S. Jun, Y. F. Zhang, Reproducing kernel particle methods,
474 International Journal for Numerical Methods in Fluids 20 (1995) 1081–
475 1106.
- 476 [5] J. S. Chen, M. Hillman, S. W. Chi, Meshfree methods: Progress made after
477 20 Years, Journal of Engineering Mechanics 143 (2017) 04017001.
- 478 [6] P. Krysl, T. Belytschko, Analysis of thin shells by the Element-Free
479 Galerkin method, International Journal of Solids and Structures 33 (1996)
480 3057–3080.
- 481 [7] G. R. Liu, Meshfree Methods: Moving Beyond the Finite Element Method,
482 Second Edition, Crc Press, 2009.
- 483 [8] X. Zhang, K. Z. Song, M. W. Lu, X. Liu, Meshless methods based on
484 collocation with radial basis functions, Computational Mechanics 26 (2000)
485 333–343.
- 486 [9] D. Millán, A. Rosolen, M. Arroyo, Thin shell analysis from scattered points
487 with maximum-entropy approximants, International Journal for Numerical
488 Methods in Engineering 85 (2011) 723–751.
- 489 [10] L. Wang, M. Hu, Z. Zhong, F. Yang, Stabilized Lagrange Interpolation
490 Collocation Method: A meshfree method incorporating the advantages of
491 finite element method, Computer Methods in Applied Mechanics and En-
492 gineering 404 (2023) 115780.
- 493 [11] P. Suchde, T. Jacquemin, O. Davydov, Point Cloud Generation for Mesh-
494 free Methods: An Overview, Archives of Computational Methods in Engi-
495 neering 30 (2022) 889–915.
- 496 [12] L. Deng, D. Wang, An accuracy analysis framework for meshfree collocation
497 methods with particular emphasis on boundary effects, Computer Methods
498 in Applied Mechanics and Engineering 404 (2023) 115782.
- 499 [13] J. Wang, M. Hillman, Upwind reproducing kernel collocation method for
500 convection-dominated problems, Computer Methods in Applied Mechanics
501 and Engineering 420 (2024) 116711.

- 502 [14] S. Fernández-Méndez, A. Huerta, Imposing essential boundary conditions
503 in mesh-free methods, *Computer Methods in Applied Mechanics and En-*
504 *gineering* 193 (2004) 1257–1275.
- 505 [15] X. Li, Error estimates for the moving least-square approximation and the
506 element-free Galerkin method in n-dimensional spaces, *Applied Numerical*
507 *Mathematics* 99 (2016) 77–97.
- 508 [16] J. Wu, D. Wang, An accuracy analysis of Galerkin meshfree methods ac-
509 counting for numerical integration, *Computer Methods in Applied Mechan-*
510 *ics and Engineering* 375 (2021) 113631.
- 511 [17] J. S. Chen, H. P. Wang, New boundary condition treatments in meshfree
512 computation of contact problems, *Computer Methods in Applied Mechan-*
513 *ics and Engineering* 187 (2000) 441–468.
- 514 [18] D. Liu, Y. M. Cheng, The interpolating element-free Galerkin (IEFG)
515 method for three-dimensional potential problems, *Engineering Analysis*
516 *with Boundary Elements* 108 (2019) 115–123.
- 517 [19] V. Ivannikov, C. Tiago, P. M. Pimenta, On the boundary conditions of the
518 geometrically nonlinear Kirchhoff–Love shell theory, *International Journal*
519 *of Solids and Structures* 51 (2014) 3101–3112.
- 520 [20] Y. Y. Lu, T. Belytschko, L. Gu, A new implementation of the element free
521 Galerkin method, *Computer Methods in Applied Mechanics and Engineer-*
522 *ing* 113 (1994) 397–414.
- 523 [21] T. Zhu, S. N. Atluri, A modified collocation method and a penalty formu-
524 lation for enforcing the essential boundary conditions in the element free
525 Galerkin method, *Computational Mechanics* 21 (1998) 211–222.
- 526 [22] S. Skatulla, C. Sansour, Essential boundary conditions in meshfree methods
527 via a modified variational principle: Applications to shell computations,
528 *Computer Assisted Mechanics and Engineering Sciences* 15 (2008) 123–142.
- 529 [23] J. S. Chen, C. T. Wu, S. Yoon, Y. You, A stabilized conforming nodal
530 integration for Galerkin mesh-free methods, *International Journal for Nu-*
531 *merical Methods in Engineering* 50 (2001) 435–466.
- 532 [24] J. S. Chen, M. Hillman, M. Rüter, An arbitrary order variationally consis-
533 tent integration for Galerkin meshfree methods, *International Journal for*
534 *Numerical Methods in Engineering* 95 (2013) 387–418.
- 535 [25] Q. Duan, X. Li, H. Zhang, T. Belytschko, Second-order accurate derivatives
536 and integration schemes for meshfree methods, *International Journal for*
537 *Numerical Methods in Engineering* 92 (2012) 399–424.

- 538 [26] D. Wang, J. Wu, An inherently consistent reproducing kernel gradient
539 smoothing framework toward efficient Galerkin meshfree formulation with
540 explicit quadrature, *Computer Methods in Applied Mechanics and Engi-*
541 *neering* 349 (2019) 628–672.
- 542 [27] J. Wang, X. Ren, A consistent projection integration for Galerkin meshfree
543 methods, *Computer Methods in Applied Mechanics and Engineering* 414
544 (2023) 116143.
- 545 [28] J. Wu, X. Wu, Y. Zhao, D. Wang, A consistent and efficient method for
546 imposing meshfree essential boundary conditions via hellinger-reissner vari-
547 ational principle., *Chinese Journal of Theoretical and Applied Mechanics*
548 54 (2022) 3283–3296.
- 549 [29] J. Wu, X. Wu, Y. Zhao, D. Wang, A rotation-free Hellinger-Reissner mesh-
550 free thin plate formulation naturally accommodating essential boundary
551 conditions, *Engineering Analysis with Boundary Elements* 154 (2023) 122–
552 140.
- 553 [30] J. Benzaken, J. A. Evans, S. F. McCormick, R. Tamstorf, Nitsche’s method
554 for linear Kirchhoff–Love shells: Formulation, error analysis, and verifica-
555 tion, *Computer Methods in Applied Mechanics and Engineering* 374 (2021)
556 113544.
- 557 [31] H. Dah-wei, A method for establishing generalized variational principle,
558 *Applied Mathematics and Mechanics* 6 (1985) 501–509.
- 559 [32] H. Du, J. Wu, D. Wang, J. Chen, A unified reproducing kernel gradient
560 smoothing Galerkin meshfree approach to strain gradient elasticity, *Com-*
561 *putational Mechanics* 70 (2022) 73–100.
- 562 [33] J. Kiendl, K. U. Bletzinger, J. Linhard, R. Wüchner, Isogeometric shell
563 analysis with Kirchhoff–Love elements, *Computer Methods in Applied Me-*
564 *chanics and Engineering* 198 (2009) 3902–3914.